Geophysical Journal International

Geophys. J. Int. (2014) **197,** 1196–1214
Advance Access publication 2014 March 22

doi: 10.1093/gji/ggu057

Correcting an acoustic wavefield for elastic effects

C. H. Chapman,[1] J. W. D. Hobro[1] and J. O. A. Robertsson[2]

[1] *Schlumberger Cambridge Research Ltd, High Cross, Madingley Road, Cambridge, CB3 0EL, England. E-mail: chchapman@hotmail.com*
[2] *Institute of Geophysics, Department of Earth Sciences, ETH-Zurich, Sonneggstrasse 5, CH-8092 Zurich, Switzerland*

Accepted 2014 February 12. Received 2014 February 10; in original form 2013 September 9

SUMMARY

Finite-difference simulations are an important tool for studying elastic and acoustic wave propagation, but remain computationally challenging for elastic waves in three dimensions. Computations for acoustic waves are significantly simpler as they require less memory and operations per grid cell, and more significantly can be performed with coarser grids, both in space and time. In this paper, we present a procedure for correcting acoustic simulations for some of the effects of elasticity, at a cost considerably less than full elastic simulations. Two models are considered: the full elastic model and an equivalent acoustic model with the same P velocity and density. In this paper, although the basic theory is presented for anisotropic elasticity, the specific examples are for an isotropic model. The simulations are performed using the finite-difference method, but the basic method could be applied to other numerical techniques. A simulation in the acoustic model is performed and treated as an approximate solution of the wave propagation in the elastic model. As the acoustic solution is known, the error to the elastic wave equations can be calculated. If extra sources equal to this error were introduced into the elastic model, then the acoustic solution would be an exact solution of the elastic wave equations. Instead, the negative of these sources is introduced into a second acoustic simulation that is used to correct the first acoustic simulation. The corrected acoustic simulation contains some of the effects of elasticity without the full cost of an elastic simulation. It does not contain any shear waves, but amplitudes of reflected P waves are approximately corrected. We expect the corrected acoustic solution to be useful in regions of space and time around a P-wave source, but to deteriorate in some regions, for example, wider angles, and later in time, or after propagation through many interfaces. In this paper, we outline the theory of the correction method, and present results for simulations in a 2-D model with a plane interface. Reflections from a plane interface are simple enough that an analytic analysis is possible, and for plane waves, we give the correction to the acoustic reflection and transmission coefficients. Finally, finite-difference calculations for plane waves are used to confirm the analytic results. Results for wave propagation in more complicated, realistic models will be presented elsewhere.

Key words: Numerical approximations and analysis; body waves; computational seismology; wave propagation.

1 INTRODUCTION

Simulating the propagation of elastic waves in realistic earth models is an important tool in many seismic applications including interpretation, imaging, reverse time migration, waveform inversion and survey design. The finite-difference method is an important tool for these simulations, as it is robust, relatively simple to implement, and provides a reasonable balance between efficiency and accuracy. However, performing computations for elastic waves in realistic, 3-D models is still computationally challenging. As a result, elastic simulations for P-wave sources are often approximated by acoustic wave propagation in a fluid model. These are considerably less expensive, both in terms of the memory and CPU requirements because of the simpler operations in each grid cell and the coarser grid allowed. In this paper, we only consider the finite-difference method for simulations, but the motivation and solution would apply to other numerical techniques. If the P-wave velocities in the acoustic and elastic models are equal, the kinematics of the P waves will be modelled correctly, but the dynamics of the P waves will only be approximate, and the shear waves will be completely unmodelled. In this paper, we describe a procedure to correct the acoustic simulation for some of the effects of elastic wave propagation. The basic theory in Sections 2, 3 and 5.1 is for an anisotropic elastic medium, but the specific applications in eqs (25)–(28), and

Sections 5.2, 6 and 7 are for an isotropic medium. Nevertheless, the method could be used in anisotropic elastic media provided the acoustic wave equation can be modified to model the kinematics of the anisotropic *qP* wave. A correction to the acoustic simulation is calculated using a second acoustic simulation that improves the dynamics of the *P*-wave propagation, but still completely omits the shear waves. We expect the corrected acoustic solution to be useful in regions of space and time around a *P*-wave source, but to deteriorate in some regions, for example, wider angles, and later in time, or after propagation through many interfaces. The overall cost is approximately twice that of the original acoustic simulation, but considerably less than an elastic simulation.

The computational cost of acoustic finite-difference simulations, both in terms of memory and CPU, is considerably less than elastic simulations for two reasons: the reduced requirements per grid cell for the simpler acoustic equations, and the coarser grid allowed, that is, the grid cells per unit volume and time interval. The reduced requirements per grid cell impact both the memory and CPU requirements. Acoustic simulations require six variables per grid cell (assuming one point per cell) for the four field variables (particle velocity, $\mathbf{v}$, and pressure, P) and two model variables (density, ρ, and P velocity, α), whereas elastic simulations require 12 variables as there are nine field variables (particle velocity, $\mathbf{v}$, and stress, $\boldsymbol{\sigma}$) and three model variables (density, ρ, and P and S velocities, α and β). The CPU requirements show a greater saving as the acoustic simulations require the calculation of only six spatial derivatives [three for the gradients of pressure in the equation of motion (8), and three for the dilatation-rate in the constitutive eq. (7)], whereas the elastic simulations require 18 spatial derivatives [nine for the gradients of stress in the equation of motion (1), and nine for the strain rates in the constitutive eq. (2)]. The other operations in the finite-difference calculations are less significant than the spatial derivatives. Although these ratios between elastic and acoustic computations are significant (approximately two for memory and three for CPU), a more significant factor is the different requirements for the grid cell size. To avoid dispersion, a certain number of gridpoints is required per wavelength. The exact number depends on the order of discrete operators used to approximate the spatial operators and the accuracy required, but the grid spacing must be proportional to the wavelengths in the simulation. Thus, the grid spacing will be controlled by the shortest wavelength or slowness velocities in the simulation. In the acoustic simulation, this will be the minimum P-wave velocity, $\alpha_{\min}$, whereas in the elastic simulation it will be the minimum S-wave velocity, $\beta_{\min}$. Thus, the ratio of the grid spacing in acoustic to elastic simulations is the ratio of these velocities, $\alpha_{\min}/\beta_{\min}$. This must apply in each spatial dimension. In addition to obtain temporal stability, the time step must be below a certain value determined by the Courant number and the ratio of the minimum to maximum velocities in the model (Robertsson & Blanch 2011), that is, $\alpha_{\min}/\alpha_{\max}$ in the acoustic model and $\beta_{\min}/\alpha_{\max}$ in the elastic model. Thus, overall, the ratio of the total number of grid cells, from both the spatial and temporal grids, in the elastic and acoustic simulations is $(\alpha_{\min}/\beta_{\min})^4$. For a Poisson solid, this is a factor of nine but for models with low shear velocity sediments, for instance near the seafloor, the number may be considerably higher. The combination of the cost per cell, with the number of cells required, makes the elastic simulations considerably more expensive than acoustic simulations, typically between two and three orders of magnitude. The above argument is based on the simplest situation, one point per grid cell and computations dominated by the spatial derivatives. The numbers are simple but not simplistic. The conclusion is robust even if the numbers are refined for more complex situations—elastic simulations are always much more expensive than acoustic simulations.

Another possible way to reduce the cost of elastic simulations is to use a finite-difference grid controlled by the P waves only and allow the dispersion of S waves. Sometimes these non-physical, inaccurate arrivals can be tolerated, but they may be confusing when the dispersed S waves generate non-physical P waves in complex models (in fact for one of the finite-difference simulations in this paper, Fig. 1, the shear waves are undersampled, but the model is simple, that is, the generated shear waves do not interact again with the interface, so they cause no confusion). In any case, the computational cost of this method is about three times an acoustic simulation (the operations per grid cell), whereas the method proposed in this paper is only about two times more expensive than an acoustic simulation.

In Section 2, we review the equations of elastodynamic and acoustic wave propagation to establish the notation used throughout the paper. Although these equations are well known, particular emphasis is placed on the introduction of sources into the equations as these are crucial to the correction procedure. Section 3 describes the correction procedure. This is an iterative procedure where the error in the elastic wave equations is used to estimate the sources required in an acoustic correction simulation to improve the approximate solution. The procedure is general and might be used to correct solutions of any wave equation using solutions of another, but in our application, we consider corrections for the isotropic elastic wave equation using solutions of the acoustic wave equation.

In Section 4, we illustrate applications of the theory for wave propagation in a model consisting of two homogeneous half-spaces. In the acoustic model, the only waves generated are the reflected and transmitted P waves—in the elastic model we have the reflected and transmitted converted S waves as well. For simplicity, the finite-difference computations are done in two dimensions. Although, in this example, the model and waves generated are very simple, the results are very encouraging and illustrate the value of the method. The computations are performed for two models: a typical sedimentary interface, and a strong interface between sediment and salt. Computations for more realistic, complex structures are published elsewhere (Hobro *et al.* 2014).

To confirm the success of the correction procedure, in the final two sections of the paper, the procedure is applied to the reflection and transmission of plane waves from a plane interface. The problem is simple and well enough understood that it can be analysed analytically to obtain expressions for the expected corrections to the reflection and transmission coefficients. These are then compared with the well-known expressions for the acoustic and elastic coefficients, and for finite-difference simulations for plane waves in one dimension. These corrections are particularly good for the reflected waves.

2 ELASTODYNAMIC THEORY

In this section, we briefly review the elastodynamic wave equations in order to introduce the notation used throughout this paper. The equation of motion and the constitutive relationships can be written

$$\rho \frac{\partial \mathbf{v}}{\partial t} - \frac{\partial \boldsymbol{\sigma}_j^{\mathrm{C}}}{\partial x_j} = \mathbf{f} - \frac{\partial \mathbf{m}_j}{\partial x_j}, \tag{1}$$

$$\frac{\partial \boldsymbol{\sigma}_j^{\mathrm{C}}}{\partial t} - \mathbf{c}_{jk} \frac{\partial \mathbf{v}}{\partial x_k} = \mathbf{0}, \tag{2}$$

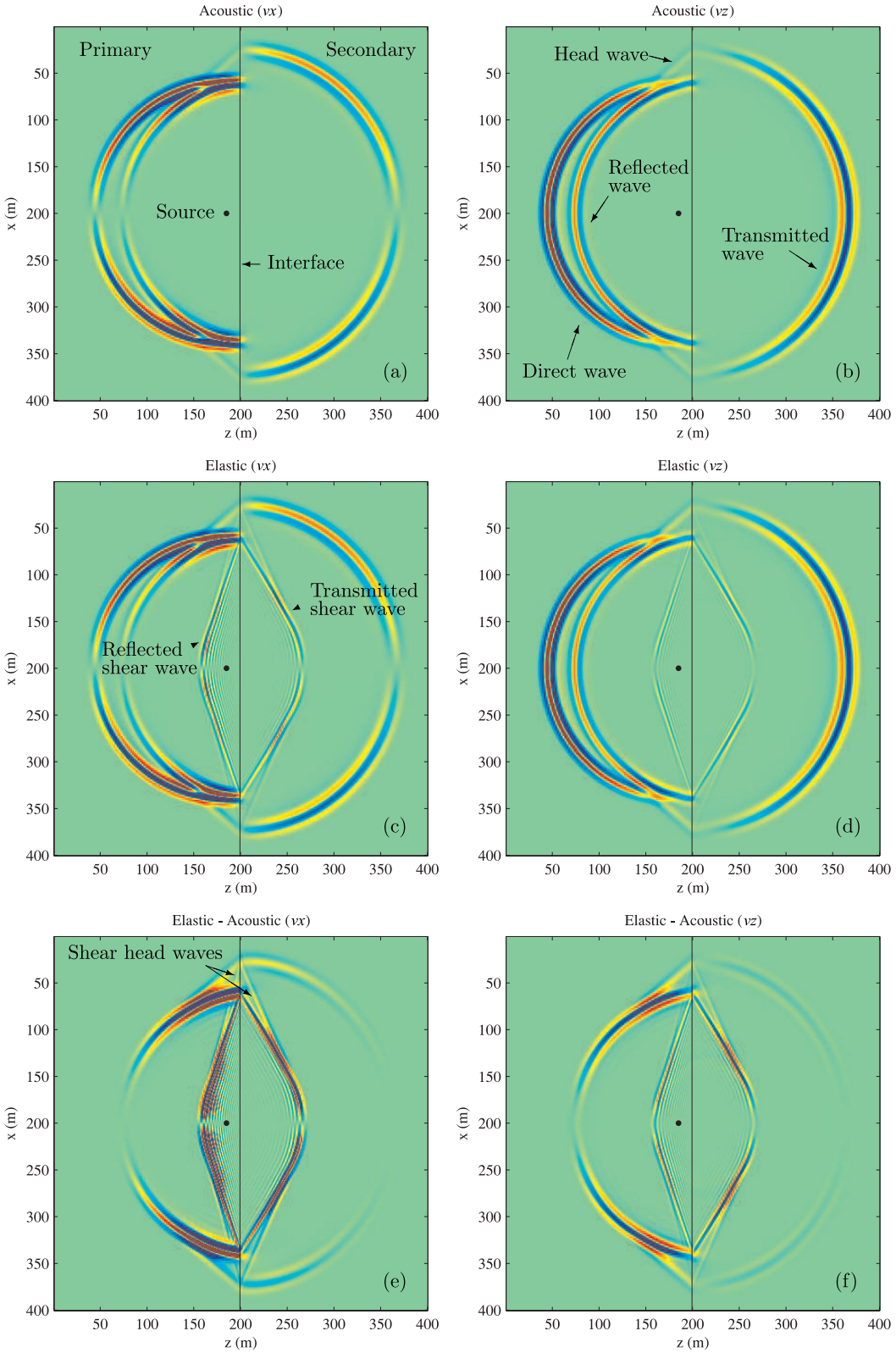

Figure 1. Wavefield snapshots in the sedimentary simulations. The subfigures on the left-hand side (a, c, e, g and i) are the x-component of particle velocity, and the subfigures on the right-hand side (b, d, f, h and j) are the z-component. The first row (a and b) is the acoustic simulation; the second row (c and d) is the elastic simulation; the third row (e and f) is the difference between the acoustic and elastic wavefields (a–d), scaled by a factor of $(10/3)$ to show the differences in P-wave amplitudes and the addition of converted S waves in the elastic results; the fourth row (g and h) is the correction to the acoustic wavefield, which approximately reproduces the differences in P-wave amplitudes plotted in (e) and (f); and, the fifth row (i and j) is the residual after the correction has been applied and plotted with the same colour scale as (e) to (h). The black line marks the critical angle within the reflected wave in subfigures (i) and (j).

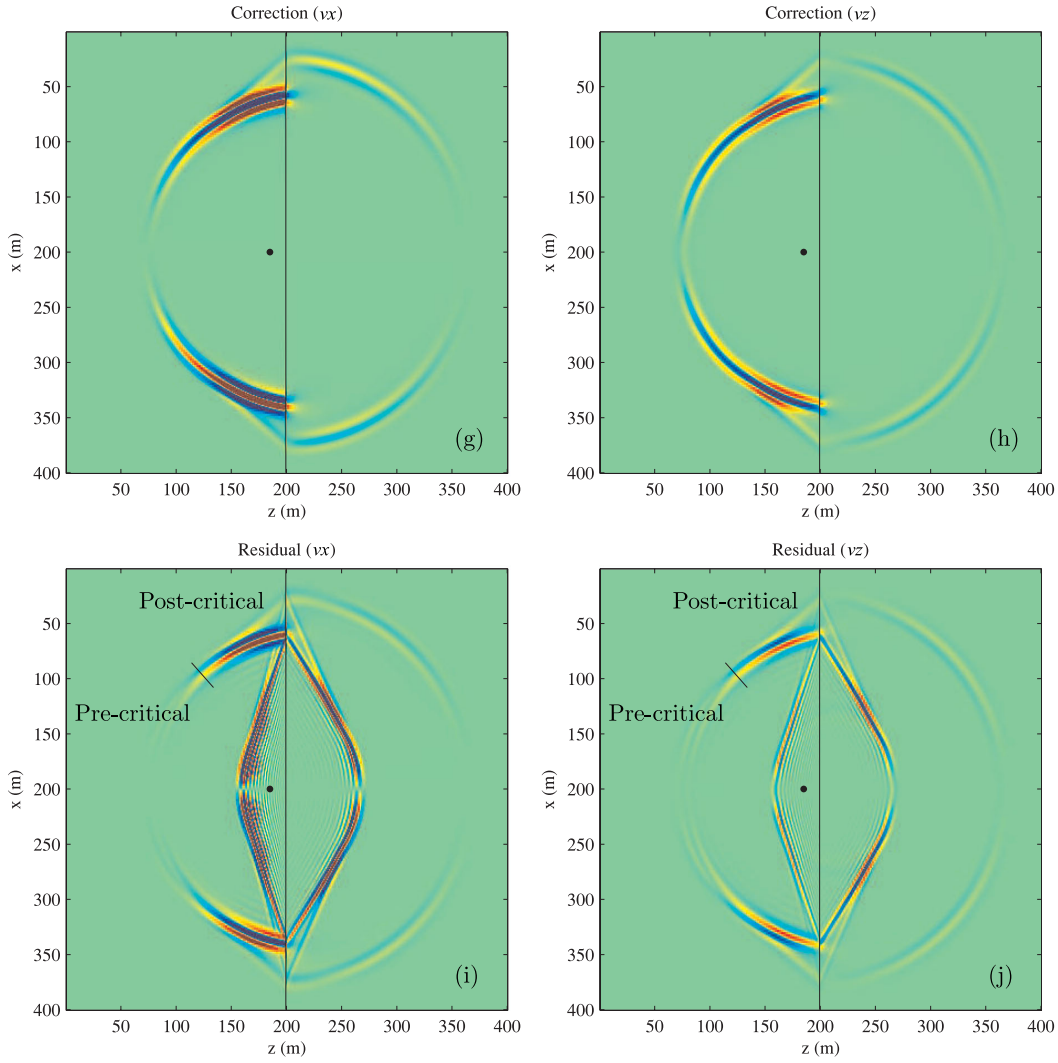

Figure 1. (*Continued.*)

where $\mathbf{v}$ is the particle velocity and $\boldsymbol{\sigma}$ the stress tensor. The traction on the jth Cartesian surface orthogonal to the jth axis is

$$\boldsymbol{\sigma}_j = \boldsymbol{\sigma}\ \hat{\boldsymbol{\imath}}_j \tag{3}$$

($\hat{\boldsymbol{\imath}}_j$ is a unit vector in the jth direction). We use Woodhouse's (1974) notation for the 3×3 matrices, $\mathbf{c}_{jk}$, of elastic stiffnesses, where $(\mathbf{c}_{jk})_{il} = c_{ijkl}$ are the elements of the fourth-order elastic stiffness tensor, and we use the Einstein summation convention. The source terms in the equation of motion (1) are the force-density vector, $\mathbf{f}$, and the moment-density tensor, $\mathbf{m}$ (both are per unit volume). As the continuum relationships (2) are taken as satisfied everywhere, we indicate by the superscript $^{\mathrm{C}}$ that the stress in these equations is the model or continuum stress not the true stress, $\boldsymbol{\sigma}$.

Normally, we take the moment-density tensor to be the stress glut (Backus & Mulcahy 1976), that is, the difference between the continuum and true stresses

$$\boldsymbol{\sigma} = \boldsymbol{\sigma}^{\mathrm{C}} - \mathbf{m}, \tag{4}$$

and the equation of motion and the constitutive relationships can be rewritten

$$\rho \frac{\partial \mathbf{v}}{\partial t} - \frac{\partial \boldsymbol{\sigma}_j}{\partial x_j} = \mathbf{f}, \tag{5}$$

$$\frac{\partial \boldsymbol{\sigma}_j}{\partial t} - \mathbf{c}_{jk} \frac{\partial \mathbf{v}}{\partial x_k} = -\frac{\partial \mathbf{m}_j}{\partial t}. \tag{6}$$

As Backus & Mulcahy (1976) noted, other definitions of the moment-density tensor are possible, which result in silent sources, for example, the moment-density, force-equivalent vector in eq. (1) is zero, that is, $-\partial_j \mathbf{m}_j = \mathbf{0}$ even when $\mathbf{m} \neq \mathbf{0}$. We will encounter such a situation later (28).

In a fluid, the constitutive relationships (2) reduces to

$$\frac{\partial P^{\mathrm{C}}}{\partial t} + \kappa \nabla \cdot \mathbf{v} = 0, \tag{7}$$

where P^{C} is the continuum pressure and κ is the bulk modulus. It is important to note that in a fluid, a general moment-density source must be introduced through its force-equivalent vector in the equation of motion

$$\rho \frac{\partial \mathbf{v}}{\partial t} + \nabla P^{\mathrm{C}} = \mathbf{f} - \frac{\partial \mathbf{m}_j}{\partial x_j}, \tag{8}$$

and not in the constitutive relationships (unless we retain the full stress tensor), because in the source region (where $\mathbf{m} \neq \mathbf{0}$), the true stress may not be the negative of an isotropic pressure, that is, sources other than pressure sources are possible in a fluid. Again, we will encounter such a situation later.

Although finite-difference calculations are usually performed using a discrete version of the first-order eqs (5) and (6), which reduce naturally to the staggered-grid, velocity–stress formulation of Virieux (1986), the stress can be eliminated between eqs (1) and (2), or (5) and (6), to obtain the second-order wave equation

$$\mathcal{L}(\mathbf{u}) = \rho \frac{\partial^2 \mathbf{u}}{\partial t^2} - \frac{\partial}{\partial x_j}\left(\mathbf{c}_{jk}\frac{\partial \mathbf{u}}{\partial x_k}\right) = \mathbf{f} - \frac{\partial \mathbf{m}_j}{\partial x_j}, \tag{9}$$

where we introduce the shorthand notation $\mathcal{L}(\mathbf{u})$ for the second-order operator and $\mathbf{u}$ is the particle displacement. In a fluid, this will be

$$\mathcal{L}(\mathbf{u}) = \rho \frac{\partial^2 \mathbf{u}}{\partial t^2} - \nabla(\kappa \nabla \cdot \mathbf{u}) = \mathbf{f} - \frac{\partial \mathbf{m}_j}{\partial x_j}. \tag{10}$$

In these wave equations, the source is the force-density vector and the moment-density, force-equivalent vector. We note that for indigenous sources, that is, internal and balanced, the force-density is usually assumed to be zero and the moment-density symmetric (no force or torque sources), but for non-indigenous sources, that is, external and unbalanced, non-zero forces and torques (asymmetric moment-density tensors) are possible.

3 THE ITERATIVE CORRECTION SCHEME

Although the first-order partial differential system, (5) and (6), corresponds closely to the numerical implementation of finite-difference codes and is convenient for analytic investigations, it is not immediately suitable for investigating the correction scheme. Instead, we use the second-order wave eq. (9) or (10). The correction scheme depends on the residual being small, that is, for two different models we require the difference in the solutions to be small. Comparing acoustic and elastic models for a *P*-wave source, we expect the differences between the acoustic and elastic particle displacements to be small, at least in a limited spatial and temporal domain (which might exclude critical angles, long-time reverberations, etc.), even when the shear modulus, μ^{E}, is significant in the elastic model. While the particle displacements will be similar for the two models, the stresses will differ significantly. For an acoustic wave, the normal stresses are all equal to the negative of the hydrostatic pressure, and the shear stresses are zero. For a *P* wave in an elastic medium, the normal stresses differ and the shear stresses are non-zero. Even in a homogeneous medium, the stresses differ (an explicit example is given below for plane waves, eq. 67). Thus, we consider the second-order wave eq. (9) or (10), which only involves the particle displacement as we expect it to be similar in the two models.

Let us consider two models, represented by operators $\mathcal{L}^{\mathrm{A}}$ and $\mathcal{L}^{\mathrm{E}}$ with solutions $\mathbf{u}^{\mathrm{A}}$ and $\mathbf{u}^{\mathrm{E}}$, that is,

$$\mathcal{L}^{\mathrm{A}}(\mathbf{u}^{\mathrm{A}}) = \mathbf{f}, \tag{11}$$

$$\mathcal{L}^{\mathrm{E}}(\mathbf{u}^{\mathrm{E}}) = \mathbf{f}, \tag{12}$$

where, for simplicity, we take the source identical in the two models, and for brevity we include any moment-density source as its force-equivalent in $\mathbf{f}$. In our application, model A will be an acoustic model, and model E an elastic model designed so the kinematic *P* properties are the same. However, the method is more general and could be used for any two models that differ but have the same approximate solution, that is, model A would be an approximation to the exact model E. Formally, we require

$$\left|\mathbf{u}^{\mathrm{E}} - \mathbf{u}^{\mathrm{A}}\right| \ll \left|\mathbf{u}^{\mathrm{A}}\right|, \tag{13}$$

which imposes limits on the differences in the elastic parameters and the maximum frequency. We only expect this condition (13) to be true in limited spatial and temporal domains.

Suppose we know the exact solution, $\mathbf{u}^{\mathrm{A}}$, in model A (11). We use this as an approximate solution (pre-conditioner) of the second equation for model E (12). Then

$$\mathcal{L}^{\mathrm{E}}(\mathbf{u}^{\mathrm{A}}) = \mathbf{f} + (\mathcal{L}^{\mathrm{E}} - \mathcal{L}^{\mathrm{A}})(\mathbf{u}^{\mathrm{A}}) = \mathbf{f} + \delta\mathcal{L}(\mathbf{u}^{\mathrm{A}}), \tag{14}$$

say, where we have defined the difference operator, $\delta\mathcal{L} = \mathcal{L}^{\mathrm{E}} - \mathcal{L}^{\mathrm{A}}$, such that

$$\delta\mathcal{L}(\mathbf{u}^{\mathrm{A}}) = -\frac{\partial}{\partial x_j}\left(\delta\mathbf{c}_{jk}\frac{\partial \mathbf{u}^{\mathrm{A}}}{\partial x_k}\right) = -\delta\mathbf{f}, \tag{15}$$

say, with

$$\delta\mathbf{c}_{jk} = \mathbf{c}^{\mathrm{E}}_{jk} - \mathbf{c}^{\mathrm{A}}_{jk}. \tag{16}$$

Expression (15) is an error in the second wave equation (E) when the solution of the first wave equation (A) is substituted. As the solution of the first wave equation is known, the error can be considered known and can be calculated. It plays the role of an extra source term, $-\delta\mathbf{f}$, in the second wave equation. With the total source, $\mathbf{f} - \delta\mathbf{f}$, the solution of the first wave equation, $\mathbf{u}^{\mathrm{A}}$, exactly satisfies the second wave equation, (14). To obtain a better solution of the second wave equation, we consider another solution, $\delta\mathbf{u}$, of the first wave equation (A) with the 'negative' of this source term, that is

$$\mathcal{L}^{\mathrm{A}}(\delta\mathbf{u}) = \delta\mathbf{f}. \tag{17}$$

We refer to $\delta\mathbf{f}$ as the residual error source. Note that, from (15), it is equivalent to a residual moment-density error source

$$\delta\mathbf{m}_j = -\delta\mathbf{c}_{jk}\frac{\partial \mathbf{u}^{\mathrm{A}}}{\partial x_k}. \tag{18}$$

Simple algebra then shows that

$$\mathcal{L}^{\mathrm{E}}(\mathbf{u}^{\mathrm{A}} + \delta\mathbf{u}) = \mathbf{f} + \delta\mathcal{L}(\delta\mathbf{u}). \tag{19}$$

Thus, the combination

$$\mathbf{u}^{\mathrm{E}} \simeq \mathbf{u}^{\mathrm{A}} + \delta\mathbf{u} \tag{20}$$

satisfies the second wave equation with an error $\delta\mathcal{L}(\delta\mathbf{u})$. Compared with the original error, $\delta\mathbf{f}$, the difference operator acts on the correction to the acoustic solution, $\delta\mathbf{u}$, rather than the acoustic solution, $\mathbf{u}^{\mathrm{A}}$. In general, the error should be reduced. We expect it to be a second-order error, although we are unable to prove this rigorously as there will be regions in space and time where (13) is not true.

The iterative procedure for correcting the solution can be continued but probably the first iteration considered here will be the most useful and more iterations unnecessary. If the correction is not small, the convergence will likely be very poor anyway. If the velocities of the significant arrivals in the two models differ, then the iterative correction will correct the traveltimes as a Taylor expansion, that is, $\exp[\mathrm{i}\omega(T + \delta T)] = \exp(\mathrm{i}\omega T)(1 + \mathrm{i}\omega\,\delta T + \dots)$ or $f(T + \delta T) = f(T) + \delta T f'(T) + \dots$, and this is only effective at low frequencies. However, if the mismatch in kinematic properties is restricted to small regions or small-scale fluctuations, the temporal mismatch may be small enough that iterations are effective.

Implementing the iteration in a practical sense (e.g. in a finite-difference code) exploits causality. When the wave solution from the first model arrives at a point in the second model, it does not satisfy the necessary differential equations. If an 'effective' source is introduced to satisfy the equations, then this will initiate 'scattered' waves from the point. The argument is very similar to that in the theory of error Born scattering (Chapman 2004, section 10.3)

although details of the application and theory differ. The iterative procedure developed here could be obtained by applying Born scattering theory to the elastic wave equation, where the perturbation is the shear modulus, and using the force-equivalent for the scattering sources so the elastic Green's functions can be replaced by the acoustic Green's functions. In a finite-difference code, at each time step, errors are calculated using the second model, and put back into the first model as residual sources. Negating the effect by introducing the negative of the error in the first model —the residual sources—improves the solution.

Although it has been necessary to pose the correction scheme using the second-order operator, $\mathcal{L}$, for numerical and analytic purposes we use the first-order scheme, (8) and (7). Thus, for the acoustic solution, we solve the equations

$$\rho \frac{\partial \mathbf{v}^{\mathrm{A}}}{\partial t} + \nabla P^{\mathrm{A}} = \mathbf{f}, \tag{21}$$

$$\frac{\partial P^{\mathrm{A}}}{\partial t} + \kappa^{\mathrm{A}} \nabla \cdot \mathbf{v}^{\mathrm{A}} = 0 \tag{22}$$

(the zeroth iteration), and for the correction we solve

$$\rho \frac{\partial (\delta \mathbf{v})}{\partial t} + \nabla (\delta P) = \delta \mathbf{f}, \tag{23}$$

$$\frac{\partial (\delta P)}{\partial t} + \kappa^{\mathrm{A}} \nabla \cdot (\delta \mathbf{v}) = 0 \tag{24}$$

(the first iteration), with the residual error sources (note that because we want to use the acoustic equations, the residual error sources have to be introduced through the force-equivalent, $\delta \mathbf{f}$, rather than the residual moment-density source, $\delta \mathbf{m}$ (18)). The residual error sources are calculated using (15), where for the acoustic-isotropic elastic systems we have simply

$$\delta \mathbf{c}_{11} = \mu^{\mathrm{E}} \begin{pmatrix} 0 & 0 & 0 \\ 0 & 1 & 0 \\ 0 & 0 & 1 \end{pmatrix}, \tag{25}$$

$$\delta \mathbf{c}_{23} = \mu^{\mathrm{E}} \begin{pmatrix} 0 & 0 & 0 \\ 0 & 0 & -2 \\ 0 & 1 & 0 \end{pmatrix} \tag{26}$$

plus cyclic permutations for the other matrices. Substituting in (15) and (18), this yields

$$\delta \mathbf{m} = 2\mu^{\mathrm{E}} (\theta^{\mathrm{A}} \mathbf{I} - \mathbf{e}^{\mathrm{A}}), \tag{27}$$

$$\delta \mathbf{f} = -\nabla (\delta \mathbf{m}) = 2(\mathbf{e}^{\mathrm{A}} - \theta^{\mathrm{A}} \mathbf{I}) \cdot \nabla \mu^{\mathrm{E}} + 2\mu^{\mathrm{E}} (\nabla \cdot \mathbf{e}^{\mathrm{A}} - \nabla \theta^{\mathrm{A}}), \tag{28}$$

where $\mathbf{e}^{\mathrm{A}}$ is the strain tensor and θ^{A} the dilatation of the acoustic solution. In a homogeneous region, the first term is zero as $\nabla \mu^{\mathrm{E}} = \mathbf{0}$, and the second term is zero as the acoustic wave is purely dilatational. Thus, the residual error source is only non-zero in inhomogeneous regions.

4 FINITE-DIFFERENCE EXAMPLES

In this section, we present results from a series of 2-D finite-difference simulations designed to explore and illustrate the characteristics of the method described in Section 3. The finite-difference implementation uses a staggered-grid velocity–stress formulation to solve the system of first-order differential equations [(1) and (2) in the elastic case, and (7) and (8) in the acoustic case]. This follows the approaches of Virieux (1986) and Levander (1988). The method is fourth-order accurate in space and second-order accurate in time. We only considered isotropic elastic media and, for simplicity, reduce the systems to two dimensions [so the elastic system (1) and (2) has five field variables and the acoustic system (8) and (7) only three]. Simple periodic boundary conditions were applied at the edges (i.e. a wave propagating towards the edge of the grid will continue to propagate into the grid on its opposite edge) as we are only interested in early arrivals.

We implemented three versions of the code:

(1) acoustic wave propagation, eqs (21) and (22);
(2) isotropic elastic wave propagation, eqs (1) and (2);
(3) the correction method, eqs (23) and (24) with (28) to calculate the residual sources.

The correction method was implemented as a sequence of three steps:

(1) Compute a full acoustic finite-difference simulation using the same density and *P*-wave velocity as in the elastic model, with a source at a chosen location. Record the particle velocities at all time steps in pre-defined regions in which material properties change abruptly. To avoid the necessity of recording particle velocities at all time steps, the second simulation can be run simultaneously with the first;
(2) Compute the residual source terms that are due to differences in the acoustic and elastic constitutive relations from the stored particle velocities;
(3) Carry out a second full acoustic finite-difference simulation (the 'correction simulation'), this time without exciting the original source. Instead the source terms computed in the previous step are excited.

As we remarked above following eq. (28), the residual source terms are only non-zero in inhomogeneous regions or where the material properties change discontinuously. If the entire model is inhomogeneous, the computational costs will increase due to the overhead of calculating the source term everywhere (from twice to perhaps three times an acoustic simulation). Normally, this cost can be avoided if large parts of the model are homogeneous or by ignoring the residual error source if they are below a prescribed cut-off (residual sources distributed throughout inhomogeneous regions usually do not produce coherent arrivals—only when the residual sources are concentrated on 'surfaces' are coherent arrivals produced). All tests used a Ricker wavelet source function with a central frequency of 100 Hz (i.e. with a maximum frequency of approximately 200 Hz).

4.1 Half-space models

To study the behaviour of the method at a simple interface, we tested the finite-difference implementation described above on two isotropic half-space models. The half-space models each consist of a pair of homogeneous half-spaces with different seismic properties separated by a planar interface. The seismic parameters in the two models (Table 1) were chosen to represent a strong sedimentary contrast and a top-salt contrast. The simulations were designed to allow examination of the fundamental characteristics of the correction method for these two models and to allow analytic comparisons (Sections 6 and 7). In each case, a pressure point source was excited

Table 1. Seismic parameters for the two half-space models.

Model	Medium	*P*-wave velocity	*S*-wave velocity	Density
Sediment	Primary	$1500\,\mathrm{m\,s^{-1}}$	$500\,\mathrm{m\,s^{-1}}$	$1000\,\mathrm{kg\,m^{-3}}$
	Secondary	$2000\,\mathrm{m\,s^{-1}}$	$800\,\mathrm{m\,s^{-1}}$	$1500\,\mathrm{kg\,m^{-3}}$
Top-salt	Primary	$1900\,\mathrm{m\,s^{-1}}$	$800\,\mathrm{m\,s^{-1}}$	$2000\,\mathrm{kg\,m^{-3}}$
	Secondary	$4500\,\mathrm{m\,s^{-1}}$	$2100\,\mathrm{m\,s^{-1}}$	$2100\,\mathrm{kg\,m^{-3}}$

in the primary medium close enough to the interface to allow the wavefield to be observed over a wide range of angles of incidence, including the full pre-critical wavefield, post-critical reflections and head waves.

4.1.1 Strong sedimentary contrast

The strong sedimentary contrast model was designed to test the characteristics of the correction method in an example containing a relatively large sedimentary contrast. The model is 400 m × 400 m in size, with a single planar interface separating the primary and secondary media (Fig. 1). The grid spacing used in the finite-difference simulations was 1 m × 1 m and the time step was 0.3 ms. The grid spacing was sufficiently fine to allow *P*-wave energy to propagate without significant grid dispersion, but not fine enough to prevent significant dispersion of *S* waves. The time step was chosen to give a stable finite-difference scheme while remaining close to the stability limit. Acoustic, elastic and correction simulations were all run for 360 time steps to a maximum time of 108 ms. In the acoustic and elastic simulations, an explosive point source was excited in the primary medium 15 m from the interface. Residual source terms for the correction simulation were computed within a grid surrounding the interface that contained 400 × 10 nodes and therefore covered 2.5 per cent of the total grid. The thickness of the residual source zone needs to be chosen to include the thickness of the inhomogeneous region plus the length of the finite-difference operator. As we have used a fourth-order spatial operator, 10 nodes is somewhat generous but allows us to check that the residual error terms decay to zero in the homogeneous regions. The CPU time required to compute the residual source terms within this grid was negligible compared with the CPU time consumed by the acoustic simulations.

A wavefield snapshot from the acoustic simulation is presented in Figs 1(a) and (b). In this and all subsequent wavefield snapshots, the two components of particle velocity are plotted separately at the final simulation time of 108 ms. The source and interface locations are also indicated on all plots. The acoustic simulation result contains direct, reflected, transmitted and head waves. In the equivalent wavefield from the elastic simulation (Figs 1c and d), these *P*-wave arrivals are all visible and the wavefield additionally contains reflected and transmitted *S* waves (which are dispersed). The difference between these two results is plotted in Figs 1(e) and (f) scaled by a factor of (10/3) to show the differences. This wavefield consists of the differences in amplitude in the reflected, transmitted and head waves and also contains the complete shear wavefield (reflected, transmitted and head waves). In the reflected and transmitted *P* waves, the amplitude of the difference increases with angle of incidence from zero at normal incidence. The most significant differences in *P*-wave arrivals occur in the reflected *P* wave at wide angles. The amplitude differences are much greater in the reflected wave than in the transmitted wave.

The aim of the elastic correction method (as described in Section 3 and at the beginning of this section) is to attempt to correct the amplitudes in an acoustic simulation to bring them closer to the amplitudes of *P*-wave arrivals in an elastic simulation. We therefore expect the wavefield produced by the correction simulation to approximate the *P*-wave components of the difference wavefield plotted in Figs 1(e) and (f). The result from the correction simulation is plotted in Figs 1(g) and (h). It shows a good qualitative agreement with the *P*-wave components of the difference wavefield. The residual in the corrected acoustic wavefield is plotted in Figs 1(i) and (j). This is the difference between the corrected acoustic wavefield and the elastic wavefield. It provides an indication of the accuracy of each part of the corrected acoustic wavefield. It is equivalent to the difference between the wavefields plotted in Figs 1(e) and (f), and in Figs 1(g) and (h). A black line marks the point in the reflected *P* wave that divides pre- and post-critical reflections. The residual is small in the pre-critical reflected wavefield and throughout the transmitted wavefield. However, in the post-critical reflection it increases at very wide angles to a level that is comparable with the amplitude of the converted *S* wave. Figs 1(e)–(j) are all plotted using the same magnified colour scale designed to emphasize small differences in the original particle-velocity fields.

Fig. 2 contains seismograms recorded at four locations chosen to isolate the pre- and post-critical reflected waves, the transmitted wave and the head wave. Each figure contains seismograms for the acoustic, elastic and corrected acoustic simulations superimposed for comparison, for both components of particle velocity. The pre-critical reflection seismogram in Fig. 2(a) corresponds to a high incidence angle of 45° (the critical angle is 48.6°). At this angle, there is a significant difference in amplitude between the acoustic and elastic arrivals and a small but visible phase shift. There is no phase shift between the exact acoustic and plane wave elastic solutions. The existence of significant phase shifts between the acoustic and elastic arrivals in these point-source simulations reminds us that comparisons between plane wave theory and point-source simulations must be made with care. The corrected acoustic wave accounts for the amplitude and phase differences very well. The dispersed *S*-wave arrival is also visible in the elastic seismograms. In the post-critical reflection seismograms (Fig. 2b), the phase component of the correction is still good although the amplitude of the correction is too high, generating a post-critical residual that is in antiphase with the required correction (*cf.* Figs 1e and f, and i and j). This pattern is repeated in the transmitted wavefield (Fig. 2c) although in this case the differences between the three seismograms (acoustic, elastic and corrected acoustic) are much smaller. The dispersed *S*-wave arrival is visible once again in these plots. For the head wave (Fig. 2d), all three seismograms are in phase (this is not surprising because the head wave is a plane wave) and a reasonable amplitude correction has been achieved, although not as good a correction as in the pre-critical reflected arrival.

Overall, these results offer a promising degree of validation for the use of this method for simulating the effects of elasticity on *P*-wave arrivals at low cost in sedimentary models. When applied to this relatively large sedimentary contrast, the transmitted and pre-critical reflected waves have been corrected with an impressive degree of accuracy. Even in the post-critical reflected wavefield where the residual is largest, a good phase correction has been achieved and the corrected acoustic waveform offers an improved approximation to the elastic result.

4.1.2 Top-salt contrast

The top-salt model contains an interface with a much larger contrast in seismic properties. It is designed to simulate a typical change

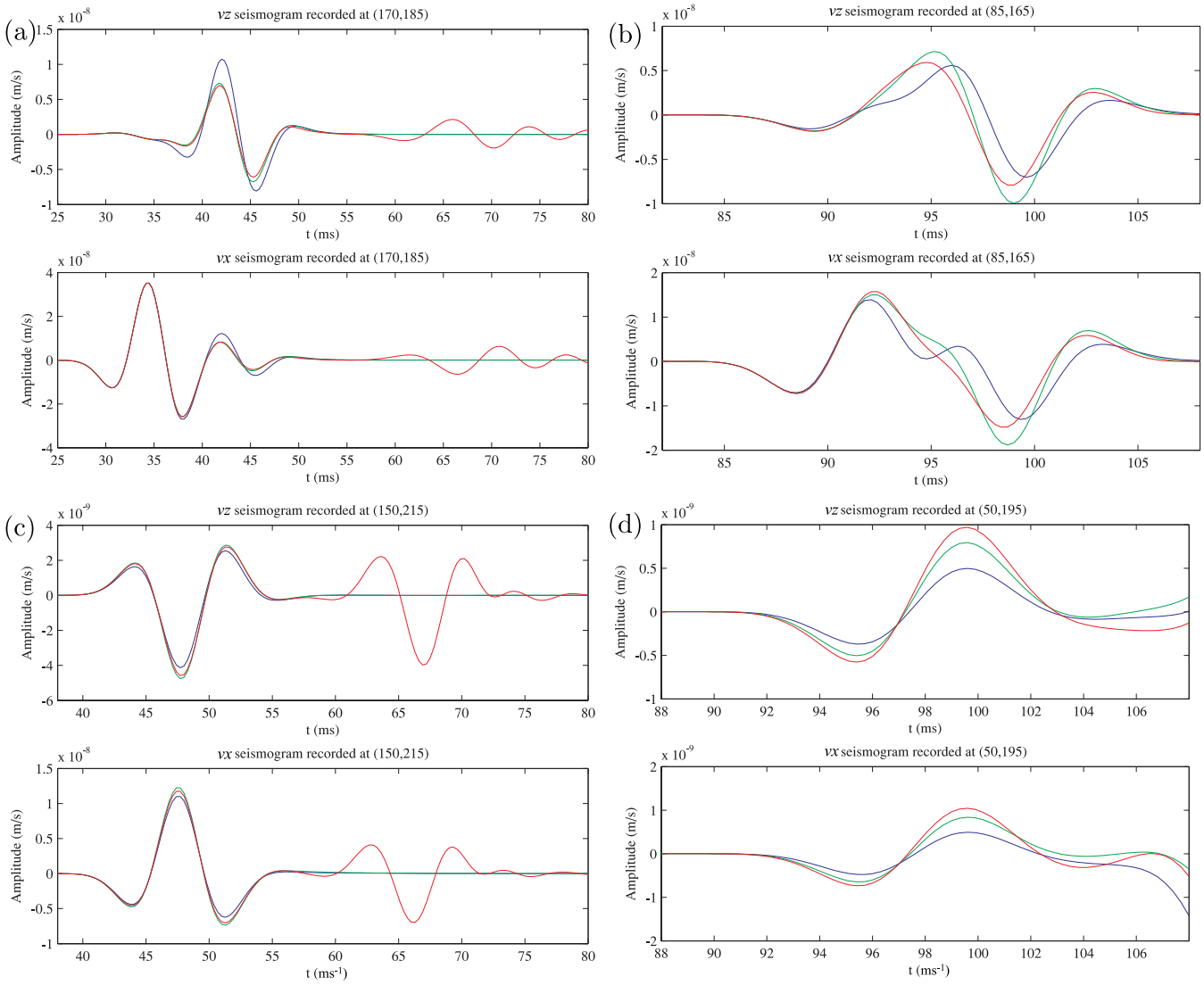

Figure 2. Particle-velocity seismograms at four locations. In each pair, the upper figure is the z-component of the particle velocity and the lower subfigure is the x-component. The acoustic seismograms are blue, the elastic red and the corrected acoustic green. Subfigure (a) is recorded at location (170, 185) corresponding to a pre-critical reflection at incident angle of 45°; subfigure (b) is recorded at location (85, 165) corresponding to a post-critical reflection at incident angle of 66.5°; subfigure (c) is recorded at location (150, 215) corresponding to a transmission with an incident angle of 43.8° and, subfigure (d) is recorded at location (50, 195) for the head wave.

in the seismic medium across the top of a salt body in shallow sedimentary rock. The model presents a significant challenge to the method presented here. This is because wave propagation across such a large contrast is likely to violate the fundamental assumption in the method (13) that the particle-velocity fields in an acoustic and elastic simulation are similar enough to allow the acoustic wavefield solution to estimate a good correction towards the elastic wavefield solution.

The model is 300 m × 440 m in size, with a single planar interface separating the primary and secondary media (Fig. 3). The grid spacing used in the finite-difference simulation was 1 m × 1 m and the time step was 0.13 ms. The grid spacing was sufficiently fine to allow *P*- and *S*-wave energy to propagate without significant grid dispersion. The time step was chosen to give a stable finite-difference scheme while remaining close to the stability limit. Acoustic, elastic and correction simulations were all run for 460 time steps to a maximum time of 61.3 ms. In the acoustic and elastic simulations, an explosive point source was excited in the primary medium 30 m from the interface. Source terms for the correction simulation were computed within a grid surrounding the interface which contained 300 × 10 nodes and, therefore, covered 2.3 per cent of the total grid (the zone of 10 nodes was chosen as in the first model). The CPU time required to compute the source terms within this grid was negligible compared with the CPU time consumed by the acoustic simulations.

A wavefield snapshot from the acoustic simulation is presented in Figs 3(a) and (b). As in the previous example, all wavefield snapshots are plotted at the final simulation time. The same range of wavefield components can be seen in Figs 3(a)–(d) as in the sedimentary case. In the difference plot [Figs 3e and f, again scaled by a factor (10/3)], the same pattern exists as in the equivalent sedimentary result (Figs 1e and f), although larger differences can be seen over a wider range of angles in the reflected *P*-wave arrival.

As in the sedimentary case, the correction simulation result (Figs 3g and h) shows a good qualitative agreement with the *P*-wave components of the difference wavefield. However, the residual in

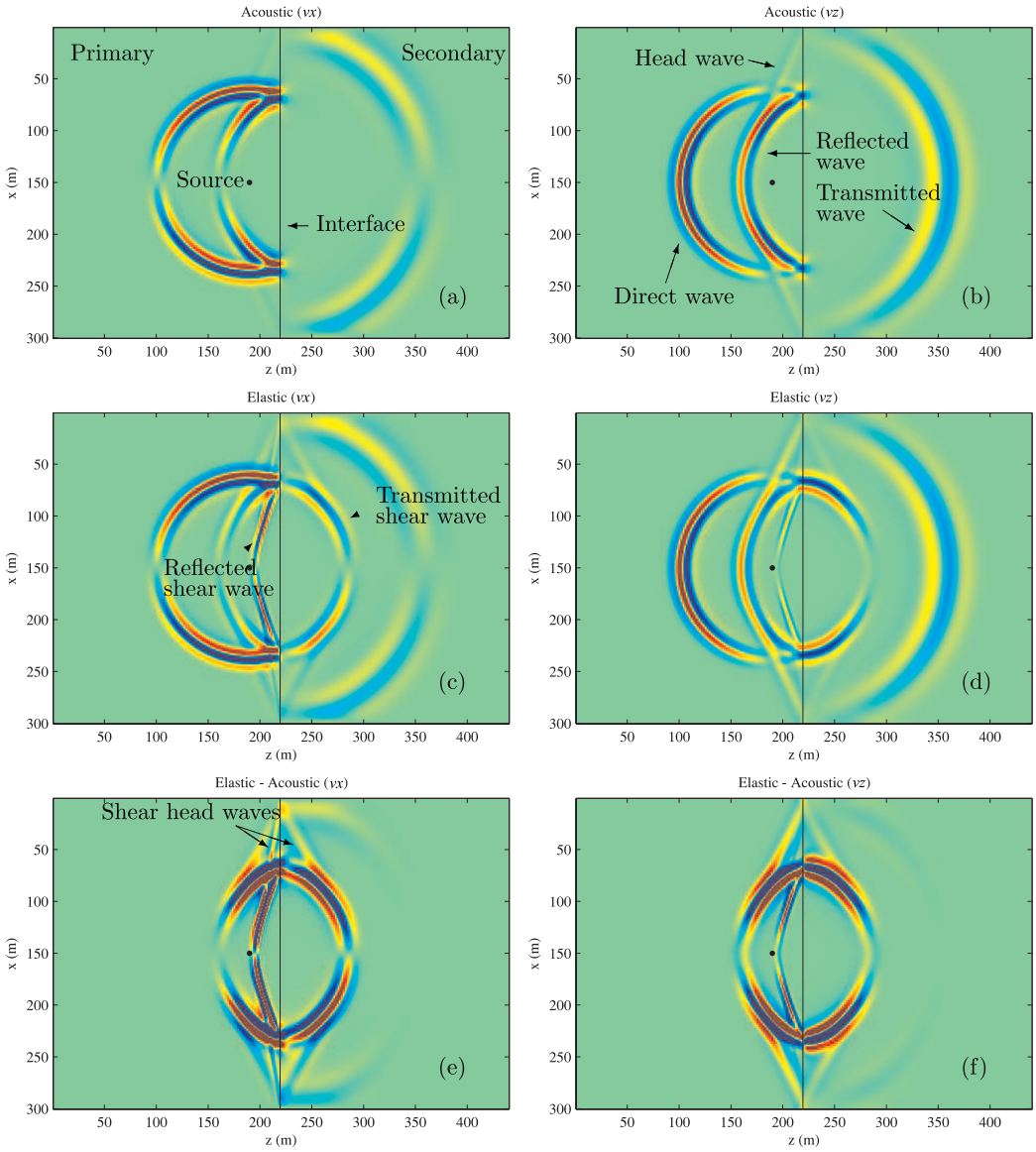

Figure 3. As Fig. 1 but for the top-salt simulations.

the *P*-wave reflection (Figs 3i and j) grows to be much larger over a wider range of angles than in the sedimentary case. The larger contrast in seismic properties has both increased the residual at post-critical angles and reduced the critical angle at which it starts to become significant. These factors together increase the overall error in the corrected acoustic wavefield significantly.

Fig. 4 contains seismograms recorded at four locations equivalent to those presented for the sedimentary example. In the pre-critical reflection seismogram (Fig. 4a), which was recorded close to the critical angle, the correction accounts well for the amplitude difference between the acoustic and elastic arrivals, although a small phase error is introduced. The corrected acoustic result offers a significant improvement over the acoustic result, if not as impressive an improvement in this case as in the sedimentary example. In the post-critical reflection (Fig. 4b), the correction brings a moderate improvement in amplitude, but overcompensates for the phase shift between the acoustic and elastic waveforms, creating a significant wavefield residual (Figs 3i and j). In the transmitted wavefield, the correction overcompensates for the amplitude difference (Fig. 4c). This overcompensation is greater than in the sedimentary example but is still extremely small compared with the amplitude differences in the reflected wavefield discussed above. The head wave amplitude is partially corrected (Fig. 4d) although the phase of the elastic head wave in this example is distorted by the proximity of the shear head wave (this can be seen most clearly in Figs 3e and f).

Overall, the results from the top-salt simulation are encouraging. The contrast in seismic properties is large enough to challenge the assumptions in the correction method. However, the corrected acoustic seismograms still bring a useful improvement over the basic acoustic results, albeit over a more limited ranges of incidence angle than for sedimentary models.

5 PLANE WAVE, DIFFERENTIAL SYSTEM

In Section 4, we demonstrated with simple numerical examples that acoustic finite-difference calculations can be corrected for elastic effects using an iterative scheme (Section 3). The numerical results for correcting *P* waves reflected and transmitted by a plane interface

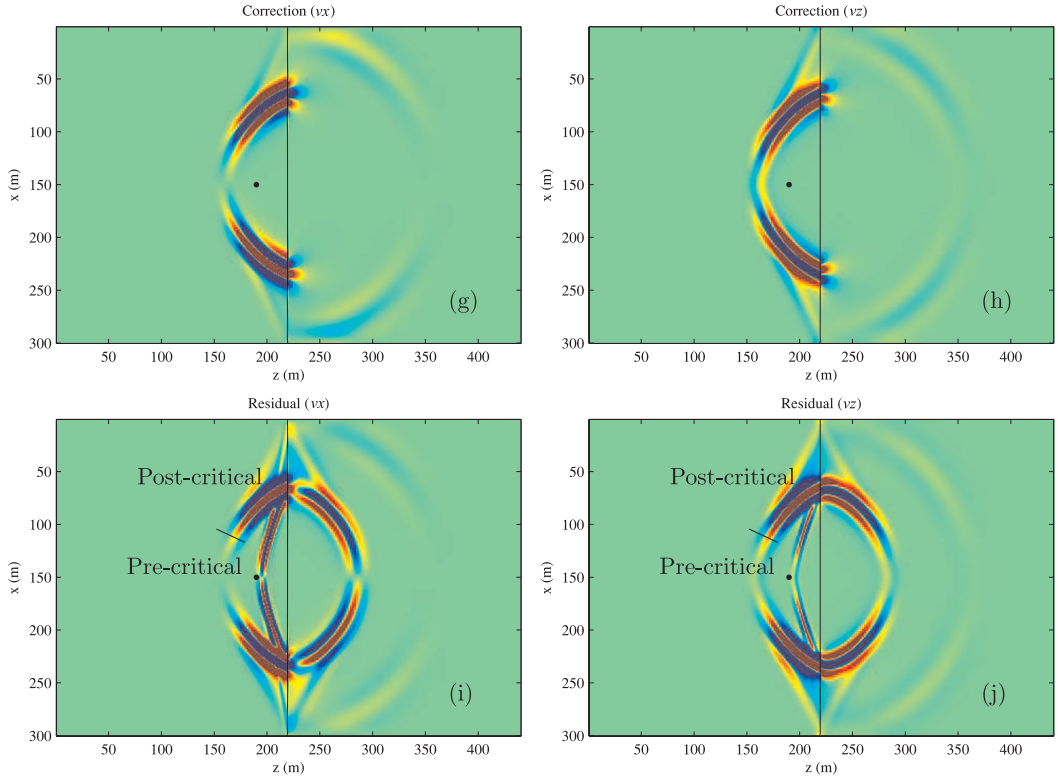

Figure 3. (*Continued.*)

are satisfactory. Of course, the shear waves reflected and transmitted at an elastic interface are not generated. Corrected finite-difference results for more complicated and realistic models are presented elsewhere (Hobro *et al.* 2014). For such models, the accuracy of the correction can only be determined by comparing with elastic finite-difference calculations. For the simple model used here in Section 4, analytic solutions are known and we can analyse the corrections in some detail. This will indicate the expected accuracy of the iterative solution. We further simplify the comparison by considering the reflection and transmission of plane waves in a 1-D model rather than the spherical waves from a point source used in Section 4.

In this section, we summarize the well-known, ordinary differential equations for plane waves in a 1-D model. The basic results are well known, but some care is required in introducing the residual sources. We also convert the ordinary differential equations into the form suitable for finite-difference calculations performed in Section 7. In Section 6, using the exact solution for the reflection and transmission of acoustic waves, we calculate the error in the elastic equations. As we are considering the analytic solutions for a discontinuous medium, the error terms will be singular at the interface. These can then be introduced into the acoustic equations, generating new waves radiated from the interface that correct the reflected and transmitted coefficients.

In Section 7, we compare the analytic results for the corrections to the exact reflection and transmission coefficients, and confirm the results using finite-difference solutions of the transformed 1-D wave equations.

5.1 One-dimensional ordinary differential equations

To investigate a reflection/transmission problem algebraically, we consider a 1-D model where the parameters vary in the $z = x_3$ direction. We refer to the positive z-direction as upgoing and the negative z-direction as downgoing. If we take the Fourier transforms with respect to coordinates x_1 and x_2 ($\partial_\nu \to \mathrm{i}\,\omega p_\nu$, $\nu = 1$ or 2 using the usual notation of Greek indices taking only the values 1 and 2) and t ($\partial_t \to -\mathrm{i}\,\omega$), then the differential systems (5) and (6) reduce to the well-known, 1-D, ordinary differential systems, (Chapman 2004, eq. 7.1.25),

$$\partial_3 \mathbf{w} = \mathrm{i}\,\omega \mathbf{A}\mathbf{w} + \mathcal{F}, \tag{29}$$

where the wavefield vector

$$\mathbf{w}(\omega, p_1, p_2, x_3) = \begin{pmatrix} \mathbf{v} \\ \boldsymbol{\sigma}_3 \end{pmatrix} \tag{30}$$

contains the (transformed) field variables, particle velocity and normal traction, that are continuous even when $\mathbf{A}$ is discontinuous at an interface. In a general anisotropic medium, the matrix $\mathbf{A}$ is given by

$$\mathbf{A}(p_1, p_2, x_3) = \begin{pmatrix} p_\nu \mathbf{Z}\,\mathbf{c}_{3\nu} & \mathbf{Z} \\ p_\eta p_\nu \left(\mathbf{c}_{\eta\nu} + \mathbf{c}_{\eta 3}\mathbf{Z}\mathbf{c}_{3\nu}\right) - \rho\,\mathbf{I} & p_\nu \mathbf{c}_{\nu 3}\mathbf{Z} \end{pmatrix}, \tag{31}$$

where $\mathbf{Z} = -\mathbf{c}_{33}^{-1}$. The source term is given by

$$\mathcal{F}(\omega, p_1, p_2, x_3) = \begin{pmatrix} \mathrm{i}\,\omega \mathbf{Z}\,\mathbf{m}_3 \\ -\mathbf{f} + \mathrm{i}\,\omega\, p_\nu (\mathbf{m}_\nu + \mathbf{c}_{\nu 3}\mathbf{Z}\,\mathbf{m}_3) \end{pmatrix} \tag{32}$$

$$\equiv \begin{pmatrix} \mathbf{0} \\ -\mathbf{f} + \mathrm{i}\,\omega\, p_\nu \mathbf{m}_\nu + \partial_3 \mathbf{m}_3 \end{pmatrix}, \tag{33}$$

where the second expression (33) follows from the previous results about equivalent forces. Although these two forms for $\mathcal{F}$ are clearly not equal, they are physically equivalent and lead to the same solution [except in the support of the source, where in the first form

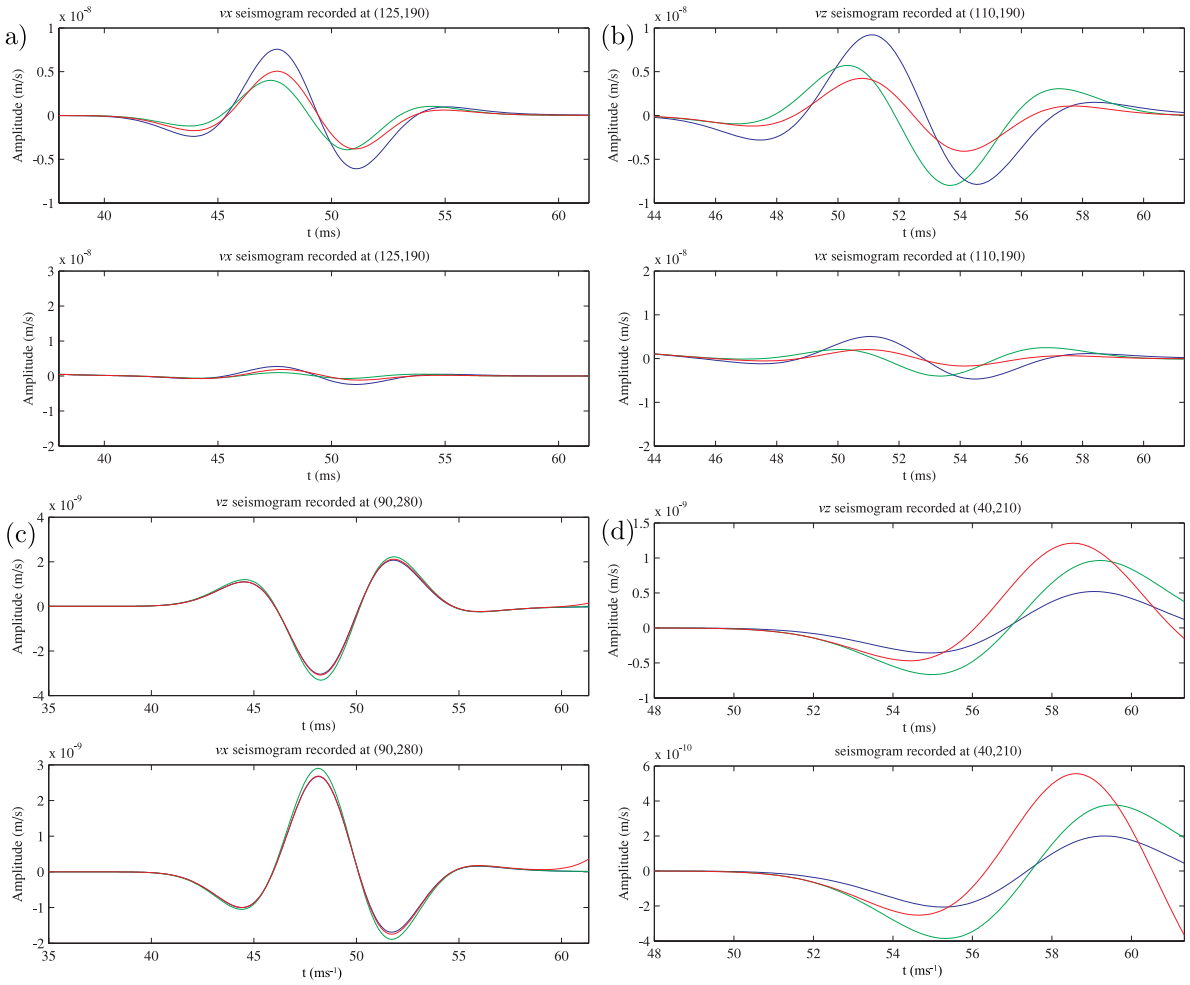

Figure 4. As Fig. 2 but for the top-salt simulations. Subfigure (a) is recorded at location (125, 190) corresponding to a pre-critical reflection at incident angle of 22.6°; subfigure (b) is recorded at location (110, 190) corresponding to a post-critical reflection at incident angle of 33.7°; subfigure (c) is recorded at location (90, 280) corresponding to a transmission with an incident angle of 15.9° and subfigure (d) is recorded at location (40, 210) for the head wave.

(32) we obtain the true traction, $\boldsymbol{\sigma}_3$, and in the second (33), the continuum traction, $\boldsymbol{\sigma}_3^{\mathrm{C}}$].

Once the solutions of the homogeneous form of equation (29) are known, the solution of the inhomogeneous eq. (29) can be found from

$$\mathbf{w}(z) = \mathbf{F}(z)\left(\mathbf{F}^{-1}(z_0)\mathbf{w}(z_0) + \int_{z_0}^{z} \mathbf{F}^{-1}(\zeta)\,\mathcal{F}(\zeta)\,\mathrm{d}\zeta\right), \tag{34}$$

where $\mathbf{F}(z)$ is a fundamental matrix of the differential system (29). The equivalence of the two forms of the source (32) and (33) depends on the equivalent forces discussed in Section 2, but also follows by simple algebra. The fundamental matrix, $\mathbf{F}$, satisfies the homogeneous form of the differential system (29), $\partial_3\mathbf{F} = \mathrm{i}\,\omega\mathbf{A}\,\mathbf{F}$, so the inverse satisfies

$$\partial_3\left(\mathbf{F}^{-1}\right) = -\mathrm{i}\,\omega\mathbf{F}^{-1}\mathbf{A}. \tag{35}$$

Considering the contribution of the final term in (33) to the integral in (34), and integrating by parts

$$\int_{z_0}^{z} \mathbf{F}^{-1}(\zeta)\begin{pmatrix}\mathbf{0}\\ \partial_3\mathbf{m}_3\end{pmatrix}\mathrm{d}\zeta = \mathbf{F}^{-1}(\zeta)\begin{pmatrix}\mathbf{0}\\ \mathbf{m}_3\end{pmatrix}\Bigg|_{z_0}^{z} - \int_{z_0}^{z} \partial_3\mathbf{F}^{-1}(\zeta)\begin{pmatrix}\mathbf{0}\\ \mathbf{m}_3\end{pmatrix}\mathrm{d}\zeta \tag{36}$$

$$= \mathrm{i}\,\omega\int_{z_0}^{z} \mathbf{F}^{-1}(\zeta)\mathbf{A}\begin{pmatrix}\mathbf{0}\\ \mathbf{m}_3\end{pmatrix}\mathrm{d}\zeta = \mathrm{i}\,\omega\int_{z_0}^{z} \mathbf{F}^{-1}(\zeta)\begin{pmatrix}\mathbf{Z}\,\mathbf{m}_3\\ p_\nu\mathbf{c}_{\nu 3}\mathbf{Z}\,\mathbf{m}_3\end{pmatrix}\mathrm{d}\zeta, \tag{37}$$

that is, the final term in (32), assuming that the source has compact support within the interval of integration. Hence, with this assumption, the two forms of $\mathcal{F}$, (32) and (33), are equivalent.

It is important to note that the differential system (29) is not directly comparable with the partial differential system (5) and (6). In particular, we cannot take the acoustic limit directly as the matrix $\mathbf{A}$ contains reciprocals of stiffnesses and the vector $\mathbf{w}$ contains components that are discontinuous at fluid interfaces. Instead, we rewrite the equation

$$\partial_t\mathbf{w} + \mathbf{A}^{-1}\partial_3\mathbf{w} = \mathbf{A}^{-1}\mathcal{F}, \tag{38}$$

taking the inverse Fourier transform with respect to frequency. The inverse matrix is

$$\mathbf{A}^{-1}(p_1, p_2, x_3) = \begin{pmatrix} -p_\nu\mathbf{X}\,\mathbf{c}_{\nu 3} & \mathbf{X} \\ p_\eta p_\nu\mathbf{c}_{3\eta}\mathbf{X}\,\mathbf{c}_{\nu 3} - \mathbf{c}_{33} & -p_\nu\mathbf{c}_{3\nu}\mathbf{X}\end{pmatrix}, \tag{39}$$

where $\mathbf{X} = (p_\eta p_\nu \mathbf{c}_{\eta\nu} - \rho\,\mathbf{I})^{-1}$. Eq. (38) is comparable with system (5) and (6) and, as we shall see, allows the acoustic limit to be taken directly, as in (7) and (8).

The results in this subsection for the 1-D, ordinary differential system are well known (e.g. Chapman 2004) except perhaps for the equivalent source representations (32) and (33), and the differential system (38) and its matrix (39).

5.2 Isotropic equations

We now specialize the system to an isotropic medium. As the system is axially symmetric, we can consider the results when $p_2 = 0$ and let $p = p_1$. As we are considering corrections to the acoustic waves, we need only consider the *P-SV* system (particle displacement in the x_1–x_3 plane), and ignore the *SH* system (particle displacement in the x_2 direction). Eliminating the *SH* system, the matrix $\mathbf{A}$ can be reduced to

$$\mathbf{A} = \begin{pmatrix} 0 & -p & -1/\mu & 0 \\ -p\lambda/\eta & 0 & 0 & -1/\eta \\ \xi p^2 - \rho & 0 & 0 & -p\lambda/\eta \\ 0 & -\rho & -p & 0 \end{pmatrix}, \tag{40}$$

where $\eta = \lambda + 2\mu$ and $\xi = 4\mu(\lambda + \mu)/\eta$. The vector $\mathbf{w}$ is

$$\mathbf{w} = \begin{pmatrix} v_1 \\ v_3 \\ \sigma_{31} \\ \sigma_{33} \end{pmatrix}, \tag{41}$$

and the source vector

$$\mathcal{F} = \begin{pmatrix} -\mathrm{i}\,\omega\, m_{13}/\mu \\ -\mathrm{i}\,\omega\, m_{33}/\eta \\ -f_1 + \mathrm{i}\,\omega p\,(m_{11} - \lambda\, m_{33}/\eta) \\ -f_3 + \mathrm{i}\,\omega p\,(m_{31} - m_{13}) \end{pmatrix} \tag{42}$$

$$\equiv \begin{pmatrix} 0 \\ 0 \\ -f_1 + \mathrm{i}\,\omega p m_{11} + \partial_3\, m_{13} \\ -f_3 + \mathrm{i}\,\omega p m_{31} + \partial_3\, m_{33} \end{pmatrix} \tag{43}$$

(where, for completeness, we have retained the possibility of non-indigenous force sources, $\mathbf{f} \neq \mathbf{0}$, and torque sources, $\mathbf{m}^{\mathrm{T}} \neq \mathbf{m}$). We reiterate that these two forms for the source vector are only equivalent if the source has compact support, that is, the contributions from the limits (36) of the source integral are zero, and that for (42), $\mathbf{w}$ contains the true stresses, and for (43), the continuum stresses.

As mentioned above, the differential system (29) with $\mathbf{A}$ given by (40) for elastic waves cannot be reduced in a straightforward manner to the acoustic system. The matrix $\mathbf{A}$ contains the reciprocal of the shear modulus and the vector $\mathbf{w}$ contains the tangential particle velocity, v_1, which is discontinuous at a fluid interface (and the zero shear-stress component, σ_{31}). However, it is straightforward to obtain the acoustic system from the transforms of eqs (7) and (8). Then (Chapman 2004, eq. 6.3.2),

$$\mathbf{A} = \begin{pmatrix} 0 & p^2/\rho - 1/\kappa \\ -\rho & 0 \end{pmatrix}, \tag{44}$$

and the wavefield vector

$$\mathbf{w} = \begin{pmatrix} v_3 \\ -P \end{pmatrix} \tag{45}$$

with the variables, normal particle velocity and pressure, that are continuous at an interface. The source vector is

$$\mathcal{F} = \begin{pmatrix} p\,(f_1 - \mathrm{i}\,\omega p m_{11} - \partial_3 m_{13})/\,\rho \\ -f_3 + \mathrm{i}\,\omega p m_{31} + \partial_3 m_{33} \end{pmatrix} \tag{46}$$

including equivalent forces as in (43). Alternative forms like (42) are not possible as field variables that may be non-zero in the support of the source, for example, shear stresses, but zero elsewhere, have been eliminated.

The specialization of (39) in isotropic media required for the finite-difference calculations in Section 7 is

$$\mathbf{A}^{-1} = \begin{pmatrix} q_{\mathrm{P}}^{-2} & 0 & 0 & 0 \\ 0 & q_{\mathrm{V}}^{-2} & 0 & 0 \\ 0 & 0 & q_{\mathrm{V}}^{-2} & 0 \\ 0 & 0 & 0 & q_{\mathrm{P}}^{-2} \end{pmatrix} \times \begin{pmatrix} 0 & p\lambda/\eta & -1/\eta & 0 \\ p & 0 & 0 & -1/\mu \\ -\rho & 0 & 0 & p \\ 0 & \xi p^2 - \rho & p\lambda/\eta & 0 \end{pmatrix}, \tag{47}$$

where we have eliminated the *SH* components and

$$q_{\mathrm{P}} = \left(\rho/\eta - p^2\right)^{1/2}, \tag{48}$$

$$q_{\mathrm{V}} = \left(\rho/\mu - p^2\right)^{1/2} \tag{49}$$

are the *P* and *SV* x_3 slowness components. In the acoustic limit, $\mu \to 0$, $q_{\mathrm{V}} \to \infty$, $\mu q_{\mathrm{V}}^2 \to \rho$ and $\xi \to 0$. The third row of $\mathbf{A}^{-1}$ is zero so $\sigma_{31} = 0$ and the third column can be ignored. The second and fourth rows and columns reduce to

$$\mathbf{A}^{-1} = \begin{pmatrix} 0 & -1/\rho \\ -\rho/q_{\mathrm{P}}^2 & 0 \end{pmatrix}, \tag{50}$$

compatible with system (44). Combining the first and fourth rows of eq. (38) gives

$$v_1 = pP/\rho, \tag{51}$$

which will be discontinuous at interfaces if the density changes.

6 ITERATIVE CORRECTIONS TO ACOUSTIC PLANE WAVE COEFFICIENTS

In this section, we use the plane wave theory from Section 5 to evaluate the corrections to the acoustic plane wave coefficients.

6.1 Homogeneous media

We now consider an interface at $z = 0$ between two homogeneous media. For instance, the density is given by

$$\rho(z) = \rho_1 H(z) + \rho_2 H(-z) = \rho_2 + [\rho\,]H(z), \tag{52}$$

where the density jump at the interface is the saltus

$$[\rho\,] = \rho(z + 0) - \rho(z - 0) = \rho_1 - \rho_2 \tag{53}$$

(for brevity, we do not include the depth variable in the saltus—all variables are continuous except at $z = 0$). The homogeneous first medium exists for $z > 0$ and the second medium for $z < 0$. The source is located in the first medium. Note that the z-axis is shifted and reversed compared with the figures in Section 4. The two models are designed so the P-wave kinematics are identical. Where variables differ, this is indicated by a superscript, that is, μ^{E}, but when they are identical, for example, density and P-wave velocity, $\alpha = \sqrt{\eta^{\mathrm{E}}/\rho} = \sqrt{\kappa^{\mathrm{A}}/\rho}$, this is omitted. We consider the case where a plane wave is incident from the first medium, travelling in the negative z-direction, indicated by a grave ($\grave{}$) accent on relevant variables, a transmitted wave propagates in the same direction into the second medium and a reflected wave propagates in the positive z-direction, indicated by an acute ($\acute{}$) accent, in the first medium (the direction of the accent suggests the propagation direction). Henceforth, the subscripts $_1$ and $_2$ are only used to indicate the media above and below the interface, and the coordinates are indicated by (x, y, z) rather than (x_1, x_2, x_3).

The plane wave solutions can be found from the eigensolutions of the matrix $\mathbf{A}$, that is,

$$\mathbf{AW} = \mathbf{Wq}, \tag{54}$$

where $\mathbf{W}$ is a matrix of the eigenvectors, and $\mathbf{q}$ the diagonal matrix of eigenvalues (Chapman 2004, section 6.3.2). We follow the convention in Chapman (2004) and order the eigenvectors first upgoing and then downgoing. Thus, for the acoustic solution, we have $\mathbf{W} = \begin{pmatrix} \acute{\mathbf{w}} & \grave{\mathbf{w}} \end{pmatrix}$ where

$$\left.\begin{matrix} \acute{\mathbf{w}} \\ \grave{\mathbf{w}} \end{matrix}\right\} = w\alpha \begin{pmatrix} \pm q \\ -\rho \end{pmatrix} \tag{55}$$

with

$$w = (2\rho\alpha^2 q)^{-1/2} \tag{56}$$

introduced to normalize the eigenvector with respect to energy flux in the z-direction (the alternative signs, $\pm q$, in the right-hand-side vector correspond to the alternative up/down eigenvectors, $\acute{\mathbf{w}}$ and $\grave{\mathbf{w}}$, on the left-hand side). We have written $q = q_{\mathrm{P}}$ (48) as we only need the P wave.

With these eigenvectors (55), we can construct the exact solution for reflection and transmission of acoustic waves at an interface, that is,

$$\mathbf{w}^{\mathrm{A}}(z) = \left(\grave{\mathbf{w}}_1 \, \mathrm{e}^{-\mathrm{i}\omega q_1 z} + \acute{\mathcal{T}}\acute{\mathbf{w}}_1 \, \mathrm{e}^{\mathrm{i}\omega q_1 z}\right) H(z) + \grave{\mathcal{T}}\grave{\mathbf{w}}_2 \, \mathrm{e}^{-\mathrm{i}\omega q_2 z} H(-z), \tag{57}$$

where

$$\acute{\mathcal{T}} = -\grave{\mathcal{T}} = (\rho_2 q_1 - \rho_1 q_2)/\Delta, \tag{58}$$

$$\acute{\mathcal{T}} = \grave{\mathcal{T}} = 2\sqrt{\rho_1\rho_2 q_1 q_2}/\Delta, \tag{59}$$

$$\Delta = \rho_2 q_1 + \rho_1 q_2 \tag{60}$$

are the reflection and transmission coefficients for acoustic waves from the interface (Chapman 2004, eqs 6.3.7–8) [we use a notation where the first accent indicates the generated wave and the second accent indicates the incident wave—the symmetry (59) depends on the normalization (56)].

The acoustic solution (57) and the transverse particle velocity (51) are substituted in elastic equation to calculate the residual sources. The most important features are the discontinuities in the transverse particle velocity and normal gradient at the interface.

6.2 Residual sources

To correct the acoustic solution (57), we must consider the residual sources (27) and (28). These can be derived from an analysis of the solution (57). The important features are the discontinuities and singularities at the interface. The particle velocity and its gradient are given by

$$\mathbf{v}^{\mathrm{A}} = \left(\grave{\mathbf{v}}_1 \, \mathrm{e}^{-\mathrm{i}\omega q_1 z} + \acute{\mathcal{T}}\acute{\mathbf{v}}_1 \, \mathrm{e}^{\mathrm{i}\omega q_1 z}\right) H(z) + \grave{\mathcal{T}}\grave{\mathbf{v}}_2 \, \mathrm{e}^{-\mathrm{i}\omega q_2 z} H(-z) \tag{61}$$

$$\simeq c \begin{pmatrix} \rho_1 \\ -\rho_1 q_2/p \end{pmatrix} - c[\rho\,] \begin{pmatrix} 1 \\ 0 \end{pmatrix} H(z), \tag{62}$$

$$\partial_z \mathbf{v}^{\mathrm{A}} = -\mathrm{i}\omega q_1 \left(\grave{\mathbf{v}}_1 \, \mathrm{e}^{-\mathrm{i}\omega q_1 z} - \acute{\mathcal{T}}\acute{\mathbf{v}}_1 \, \mathrm{e}^{\mathrm{i}\omega q_1 z}\right) H(z) - \mathrm{i}\,\omega\, q_2 \grave{\mathcal{T}}\grave{\mathbf{v}}_2 \, \mathrm{e}^{-\mathrm{i}\omega q_2 z} H(-z) - c\,[\rho\,] \begin{pmatrix} 1 \\ 0 \end{pmatrix} \delta(z) \tag{63}$$

$$\simeq \frac{\mathrm{i}\,\omega\, c\rho_1\rho_2}{p} \left\{ \frac{q_2}{\rho_2} \begin{pmatrix} -p \\ q_2 \end{pmatrix} + \begin{bmatrix} \dfrac{q^2}{\rho} \end{bmatrix} \begin{pmatrix} 0 \\ 1 \end{pmatrix} H(z) \right\} - c\,[\rho\,] \begin{pmatrix} 1 \\ 0 \end{pmatrix} \delta(z), \tag{64}$$

where, from (51) and (55),

$$\left.\begin{matrix} \acute{\mathbf{v}} \\ \grave{\mathbf{v}} \end{matrix}\right\} = w\alpha \begin{pmatrix} p \\ \pm q \end{pmatrix} \tag{65}$$

and

$$c = \frac{2p(w\alpha q)_1}{\Delta} = \frac{p}{\Delta} \left(\frac{2q_1}{\rho_1}\right)^{1/2}. \tag{66}$$

The approximations (62) and (64) describe the behaviour in the neighbourhood of the interface (for $|z|$ small compared with the wavelength or in the limit $\omega \to 0$). The transverse particle velocity is discontinuous as expected (62), unless $[\rho\,] = 0$. The equality of the gradient of the transverse component, $\partial_z v_x$, on either side of the interface is a consequence of the curl of the particle velocity being zero in a homogeneous fluid (so $\partial_z v_x = \partial_x v_z$), and the normal particle velocity (62) and therefore its transverse gradient $\partial_x v_z$ being the same on both sides of the interface. The discontinuity in the transverse component, v_x (62), gives the delta-function singularity at the interface (64).

From these results, we can calculate the residual sources. For the 2-D plane wave solutions being considered, the significant components of the residual moment-density sources (27) are

$$\delta\mathbf{m} = \begin{pmatrix} \delta m_{xx} \\ \delta m_{zz} \\ \delta m_{zx} \end{pmatrix} = 2\mu^{\mathrm{E}} \begin{pmatrix} e^{\mathrm{A}}_{zz} \\ e^{\mathrm{A}}_{xx} \\ -e^{\mathrm{A}}_{zx} \end{pmatrix} = \mu^{\mathrm{E}} \begin{pmatrix} 2\frac{\mathrm{i}}{\omega}\partial_z v^{\mathrm{A}}_z \\ -2\,p\,v^{\mathrm{A}}_x \\ p\,v^{\mathrm{A}}_z - \frac{\mathrm{i}}{\omega}\partial_z v^{\mathrm{A}}_x \end{pmatrix} \tag{67}$$

written as a vector for simplicity. With the eigensolutions (55), the corresponding residual sources in the homogeneous regions are

$$\left.\begin{matrix} \delta\acute{\mathbf{m}} \\ \delta\grave{\mathbf{m}} \end{matrix}\right\} = -2\mu^{\mathrm{E}} w\alpha \begin{pmatrix} q^2 \\ p^2 \\ \mp p\,q \end{pmatrix}, \tag{68}$$

although the equivalent-force sources are, of course, zero. With (61)–(66), we obtain

$$\delta\mathbf{m} = \left(\delta\grave{\mathbf{m}}_1\,\mathrm{e}^{-\mathrm{i}\omega q_1 z} + \grave{\acute{\mathcal{T}}}\delta\acute{\mathbf{m}}_1\,\mathrm{e}^{\mathrm{i}\omega q_1 z}\right)H(z)$$
$$+\grave{\grave{\mathcal{T}}}\delta\grave{\mathbf{m}}_2\,\mathrm{e}^{-\mathrm{i}\omega q_2 z}H(-z) + \frac{\mathrm{i}\,c}{\omega}\begin{pmatrix}0\\0\\\overline{\mu}^{\mathrm{E}}[\rho]\end{pmatrix}\delta(z) \tag{69}$$

$$\simeq -2c\rho_1\rho_2\left\{\begin{pmatrix}\frac{\mu_2^{\mathrm{E}}q_2^2}{\rho_2}\Big/\,p\\ \frac{\mu_2^{\mathrm{E}}}{\rho_2}\,p\\ \mu_2^{\mathrm{E}}\frac{q_2}{\rho_2}\end{pmatrix} + \begin{pmatrix}\left[\frac{\mu^{\mathrm{E}}q^2}{\rho}\right]\Big/\,p\\ \left[\frac{\mu^{\mathrm{E}}}{\rho}\right]p\\ \left[\mu^{\mathrm{E}}\right]\frac{q_2}{\rho_2}\end{pmatrix}H(z)\right\}$$
$$+\frac{\mathrm{i}\,c}{\omega}\begin{pmatrix}0\\0\\\overline{\mu}^{\mathrm{E}}[\rho]\end{pmatrix}\delta(z), \tag{70}$$

where $\overline{\mu}^{\mathrm{E}} = (\mu_1 + \mu_2)/2$, the mean shear modulus in the elastic solid. The delta-function term is obtained from the singularity in $\partial_z v_x^{\mathrm{A}}$ at the interface, (64) and (67). The gradient of the residual moment-density tensor is

$$\partial_z(\delta\mathbf{m}) = -\mathrm{i}\,\omega\,q_1\left(\delta\grave{\mathbf{m}}_1\,\mathrm{e}^{-\mathrm{i}\omega q_1 z} - \grave{\acute{\mathcal{T}}}\delta\acute{\mathbf{m}}_1\,\mathrm{e}^{\mathrm{i}\omega q_1 z}\right)H(z)$$
$$-\mathrm{i}\,\omega\,q_2\grave{\grave{\mathcal{T}}}\delta\grave{\mathbf{m}}_2\,\mathrm{e}^{-\mathrm{i}\omega q_2 z}H(-z)$$
$$-2c\rho_1\rho_2\begin{pmatrix}\left[\frac{\mu^{\mathrm{E}}q^2}{\rho}\right]\Big/\,p\\ \left[\frac{\mu^{\mathrm{E}}}{\rho}\right]p\\ \left[\mu^{\mathrm{E}}\right]\frac{q_2}{\rho_2}\end{pmatrix}\delta(z) + \frac{\mathrm{i}\,c}{\omega}\begin{pmatrix}0\\0\\\overline{\mu}^{\mathrm{E}}[\rho\,]\end{pmatrix}\delta'(z). \tag{71}$$

Here, we have no need to evaluate the first terms in the homogeneous regions, or their discontinuity, as we know the force-equivalent residual sources are zero in the homogeneous regions. We only need the singular terms which come directly from the discontinuity and delta function in (70).

6.3 Iterative correction

A fundamental solution of (29) is

$$\mathbf{F}(z) = \left(\mathbf{W}_1\mathrm{e}^{\mathrm{i}\omega\mathbf{q}_1 z}\right)\mathbf{Q}H(z) + \left(\mathbf{W}_2\,\mathrm{e}^{\mathrm{i}\omega\mathbf{q}_2 z}\right)H(-z), \tag{72}$$

where $\mathbf{W}_j$ are the eigenvector matrices (54) in the two media, and (Chapman 2004, eq. 6.3.22)

$$\mathbf{Q} = \mathbf{W}_1^{-1}\mathbf{W}_2. \tag{73}$$

This fundamental solution has been designed so below the interface ($z < 0$), it corresponds to the plane wave eigensolutions, $\mathbf{W}_2\exp(\mathrm{i}\,\omega\,\mathbf{q}_2 z)$, and the solution is given by just the downgoing eigenvector in $\mathbf{W}_2$. At the interface, it has been designed to be continuous as required of a fundamental solution, that is, $\mathbf{F}(0) = \mathbf{W}_2 = \mathbf{W}_1\mathbf{Q}$, whether approaching from above or below the interface. Above the interface ($z > 0$), the solution is still given by the eigensolution, $\mathbf{W}_1\exp(\mathrm{i}\,\omega\,\mathbf{q}_1 z)$, but the eigenvectors are now 'mixed' by the interface matrix $\mathbf{Q}$. The interface matrix is given by (Chapman 2004, eq. 6.3.21)

$$\mathbf{Q} = \begin{pmatrix}\acute{\mathcal{T}} - \acute{\mathcal{T}}\grave{\mathcal{T}}^{-1}\grave{\mathcal{T}} & \acute{\mathcal{T}}\grave{\mathcal{T}}^{-1}\\ -\grave{\mathcal{T}}^{-1}\grave{\mathcal{T}} & \grave{\mathcal{T}}^{-1}\end{pmatrix}. \tag{74}$$

Using this in (34) with the residual sources at the interface, we generate the particular solution excited by these sources. The solution must consist only of waves radiated away from the interface, and these give the corrections to the reflected and transmitted waves, and the coefficients. Thus,

$$\mathbf{w}(0+) = \mathbf{W}_1\begin{pmatrix}\delta\grave{\mathcal{T}}\\0\end{pmatrix}, \tag{75}$$

$$\mathbf{w}(0-) = \mathbf{W}_2\begin{pmatrix}0\\\delta\grave{\mathcal{T}}\end{pmatrix}, \tag{76}$$

where $\delta\mathcal{T}$ are the corrections to the coefficients in the acoustic model. To determine these, we need to evaluate the source integral in (34).

In the acoustic equation, we note that the force-equivalent sources (46) contain the derivative term, $\partial_z(\delta m_{zx})$ (46). As the residual moment-density source δm_{zx} (70) contains a delta function, this term is difficult to handle as it lies at an interface and contains the derivative of the delta function. In addition, the acoustic source (46) contains the inverse density $1/\rho(\zeta)$, which is also difficult to handle as it is discontinuous at the interface. Both these problems can be avoided if we could use the alternative source expressions (42) and (43), but this is only possible in an elastic medium. Therefore, we replace the acoustic medium by an elastic medium with a very small shear modulus, μ^{A} (which, for simplicity, we can take constant throughout the model). The shear waves generated are of no interest (they travel with a very small velocity) although, at the interface, they provide the required discontinuity in the transverse particle velocity. There are two advantages in using an 'elastic' acoustic model: the fundamental solution is continuous at the interface, and the residual source can be introduced using the alternative source vector either (42) or (43). Because the problem is linear in the source vector (34), we can treat terms in (70) independently. Using (70) and (71), we obtain

$$\mathcal{F}(z) = c\begin{pmatrix}\frac{\tilde{\mu}^{\mathrm{E}}}{\mu^{\mathrm{A}}}[\rho\,]\\0\\-2\rho_1 q_2[\mu^{\mathrm{E}}]\\-2p\,\rho_1\rho_2\left[\frac{\mu^{\mathrm{E}}}{\rho}\right]\end{pmatrix}\delta(z) \tag{77}$$

for the residual source vector. Note that the sources (42) or (43) only contain m_{xx}, not its derivative, so its discontinuity (70) makes no contribution to the singularity at the interface; the discontinuity in δm_{zz} (70) gives the singularity in component $\mathcal{F}_4$ through its derivative $\partial_z(\delta m_{zz})$ in (43); and the discontinuity in m_{xz} gives the singularity in component $\mathcal{F}_3$ at the interface through its derivative $\partial_z(\delta m_{xz})$ using (43), and the singularity in δm_{xz} (70) gives the singularity in component $\mathcal{F}_1$ using (42).

At the interface, the fundamental matrix needed in integral (34) is given by $\mathbf{W}_2$ (72). In the 'elastic' acoustic model, we need only consider the rows of $\mathbf{W}_2^{-1}$ appropriate for the P waves. Thus, the source integral in (34) is written

$$\mathbf{s} = \begin{pmatrix}\acute{s}\\\grave{s}\end{pmatrix} = \int_{0-}^{0+}\widetilde{\mathbf{W}}_2^{-1}\,\mathcal{F}(\zeta)\,\mathrm{d}\zeta, \tag{78}$$

where $\mathcal{F}(\zeta)$ is given by (77) and

$$\widetilde{\mathbf{W}}_2^{-1} = w_2\alpha_2\begin{pmatrix}2\mu^{\mathrm{A}}p\,q_2 & \rho_2 - 2\mu^{\mathrm{A}}p^2 & -p & -q_2\\ 2\mu^{\mathrm{A}}p\,q_2 & -\rho_2 + 2\mu^{\mathrm{A}}p^2 & p & -q_2\end{pmatrix} \tag{79}$$

from the relevant P rows in the inverse matrix $\mathbf{W}_2^{-1}$ for the 'elastic' medium (Chapman 2004, eq. 6.3.32 with 6.3.53). As $\mathcal{F}(\zeta)$ (77) only contains a delta function, the integral (78) is simple to evaluate

$$\mathbf{s} = 2cp(w\alpha q)_2 \begin{pmatrix} \bar{\mu}^{\mathrm{E}}[\rho] + \rho_1[\mu^{\mathrm{E}}] + \rho_1\rho_2\left[\frac{\mu^{\mathrm{E}}}{\rho}\right] \\ \bar{\mu}^{\mathrm{E}}[\rho] - \rho_1[\mu^{\mathrm{E}}] + \rho_1\rho_2\left[\frac{\mu^{\mathrm{E}}}{\rho}\right] \end{pmatrix}$$

$$= \frac{2p^2}{\Delta}\left(\frac{q_1q_2}{\rho_1\rho_2}\right)^{1/2}\begin{pmatrix} 4\bar{\rho} + [\rho] \\ -[\rho] \end{pmatrix}. \tag{80}$$

Note that the 'elastic' shear modulus μ^{A} has conveniently cancelled from the product of the first components (so the acoustic limit, $\mu^{\mathrm{A}} \to 0$, is trivial), and that although the residual sources arise from different stress components, in the final expression (80) all terms have the same p–dependence.

Applying the conditions (75) and (76) to (34) with (72), we obtain

$$\delta\acute{\mathcal{T}} = \left(Q_{11} - Q_{12}Q_{22}^{-1}Q_{21}\right)\acute{s} = \acute{\mathcal{T}}\acute{s}, \tag{81}$$

$$\delta\grave{\mathcal{T}} = -Q_{22}^{-1}Q_{21}\acute{s} - \grave{s} = \grave{\mathcal{T}}\acute{s} - \grave{s} \tag{82}$$

using eq. (6.3.23) in Chapman (2004) for the combinations of elements of $\mathbf{Q}$. Thus, the corrected coefficients are

$$\acute{\mathcal{T}}^{(1)} = \acute{\mathcal{T}} + \delta\acute{\mathcal{T}} = \frac{1}{\Delta}\left\{\rho_1\rho_2\left[\frac{q}{\rho}\right] + \frac{2p^2q_1q_2}{\Delta}[\mu^{\mathrm{E}}](4\bar{\rho} + [\rho])\right\}, \tag{83}$$

$$\grave{\mathcal{T}}^{(1)} = \grave{\mathcal{T}} + \delta\grave{\mathcal{T}} = \frac{2(\rho_1\rho_2q_1q_2)^{1/2}}{\Delta} \times \left\{1 - \frac{2p^2}{\Delta}[\mu^{\mathrm{E}}]\left(\rho_1\rho_2\left[\frac{q}{\rho^2}\right] + \rho_1\left[\frac{q}{\rho}\right]\right)\right\}. \tag{84}$$

In each case, the uncorrected, acoustic coefficients are given by the first term in the braces. Note that the reflection coefficient is first order in the differences between the two media as is the correction. The transmission coefficient is of order unity (it differs from unity by a term that is first order in the differences between the two media) and the correction is second order in differences between the two media.

In Section 7, we compute numerical examples of these results.

7 NUMERICAL PLANE WAVE EXAMPLES

7.1 Coefficient corrections

It remains to compare the elastic coefficients, $\acute{\mathcal{T}}_{\mathrm{PP}}$ and $\grave{\mathcal{T}}_{\mathrm{PP}}$ (Chapman 2004, eq. 6.3.60), with the corrected acoustic coefficients, $\acute{\mathcal{T}}^{(1)} = \acute{\mathcal{T}} + \delta\acute{\mathcal{T}}$ (83) and $\grave{\mathcal{T}}^{(1)} = \grave{\mathcal{T}} + \delta\grave{\mathcal{T}}$ (84), respectively. We consider the two models in Table 1. Numerical results for the sediment model are shown in Figs 5 and 6, and for the salt model in Figs 7 and 8. In both cases, the agreement between the corrected acoustic reflection coefficient and the elastic coefficient is very satisfactory. The correction is of the same order of magnitude as the coefficient, and is only slightly less accurate for the stronger contrast (although it should be stated that in both cases, the agreement is not as good beyond the critical angle. Near the critical angle the agreement is good so the correction to the head wave is satisfactory, but at larger, post-critical angles the correction is even in the wrong direction and requires further investigation). For instance, at an incident angle of 45° (as in Fig. 2a), the acoustic reflection coefficient is in error by +37 per cent compared with the elastic coefficient, while the corrected acoustic coefficient is only in error by +4.9 per cent (the choice of 45° is arbitrary but the error is small for all pre-critical angles—Fig. 5). The situation is less satisfactory for the transmission coefficient, although the fractional difference, the difference

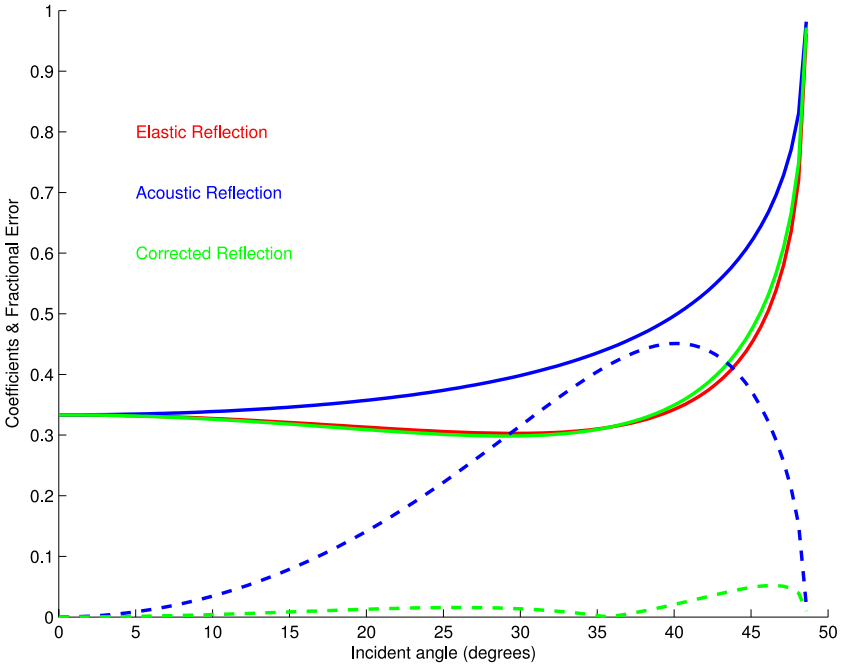

Figure 5. The elastic, acoustic and corrected reflection coefficients for the sediment model in Table 1. The colour code is the same as in Figs 2 and 4—blue for the acoustic coefficient, red for the elastic coefficient and green for the corrected acoustic coefficient. The dashed lines show the magnitude of the fractional errors of the acoustic and corrected acoustic coefficients compared with the elastic coefficient.

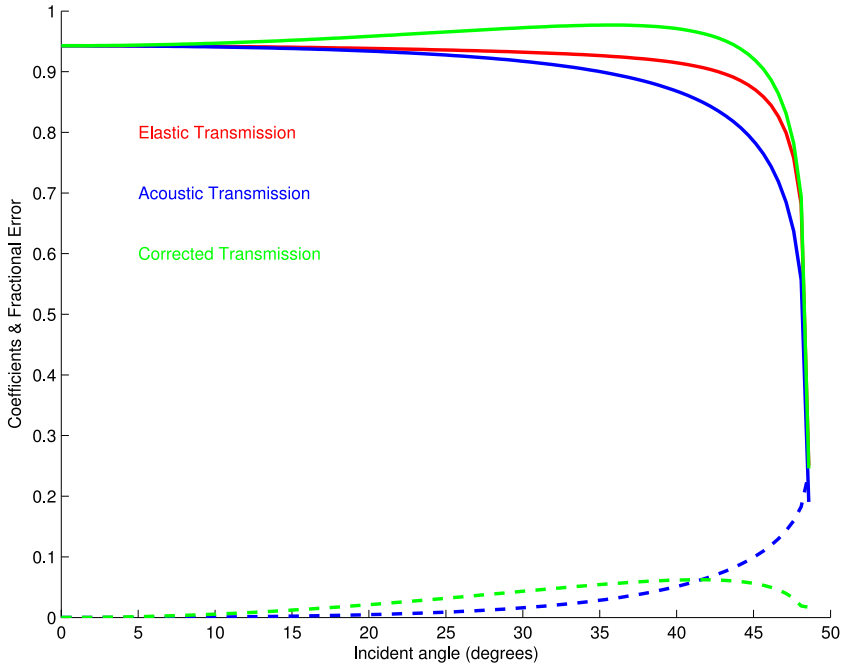

Figure 6. As Fig. 5 but for the transmission coefficients.

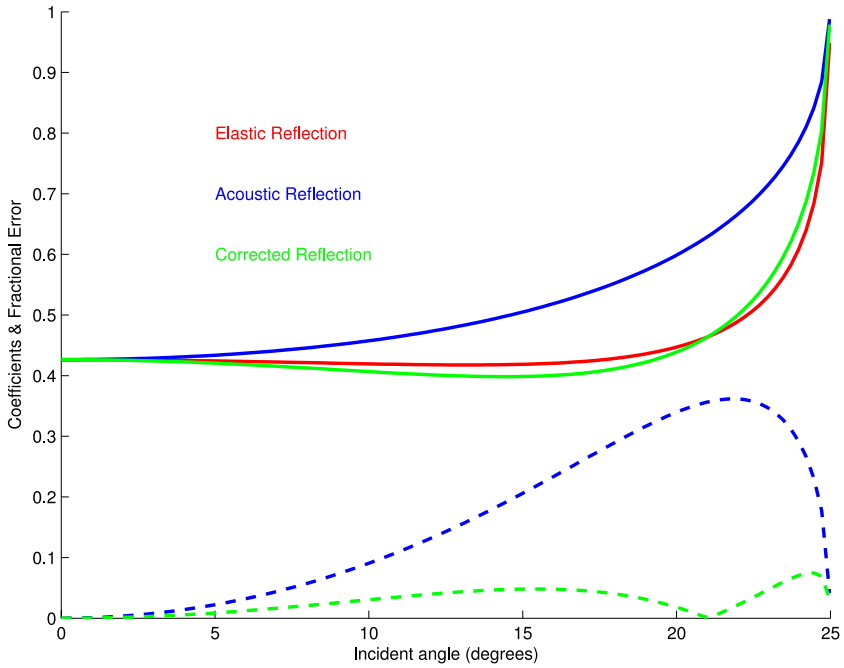

Figure 7. As Fig. 5 but for the salt model.

between the coefficients divided by the elastic coefficient, between the acoustic and elastic coefficients is much smaller. The correction to the acoustic coefficient is in the correct direction but it is too large and overshoots the elastic coefficient. At small angles, the acoustic and elastic coefficients differ little, and the correction is worse. In mid-range, the correction is about twice too large. Only near the critical angle is the corrected acoustic coefficient a better approximation to the elastic coefficient than the acoustic coefficient. Again at an incident angle of 45° (close to the angle used in Fig. 2c, which was chosen to be at a gridpoint) the acoustic transmission coefficient is in error by −9.9 per cent compared with the elastic coefficient, while the corrected acoustic coefficient is in error by +5.6 per cent.

The results in Figs 5 and 6 are in qualitative agreement with those in Section 4 (Figs 1 and 2). The results for the salt interface (Figs 7 and 8) are very similar. The accuracy of the corrected acoustic reflection coefficient (83) is remarkably good and suggests that the analytic expression might be used in other applications.

7.2 One-dimensional finite-difference calculations

We commented that the analytic expressions for the reflection and transmission coefficients are in qualitative agreement with the finite-difference results in Section 4, but a quantitative comparison is difficult due to variations in the pulse shape, etc. To compare the

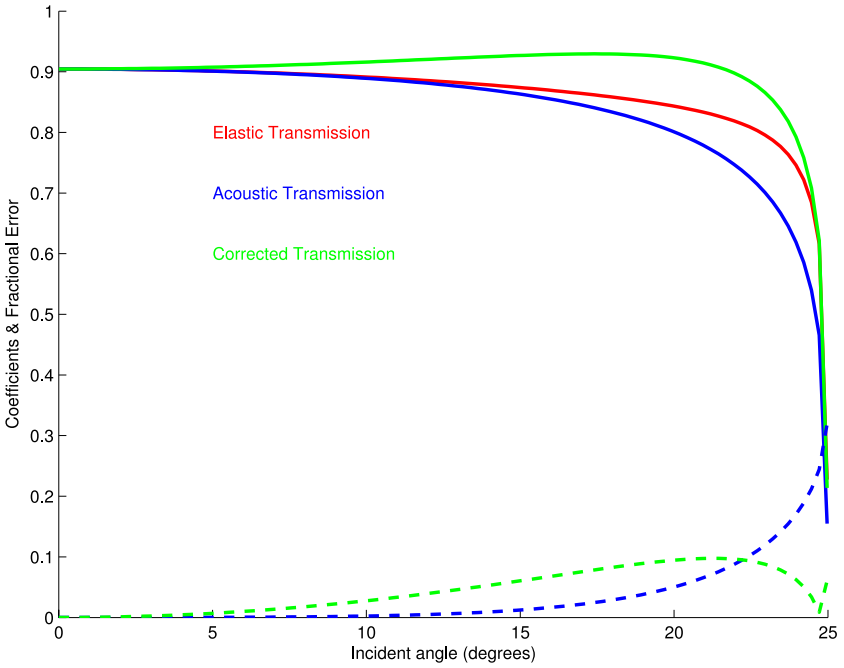

Figure 8. As Fig. 6 but for the salt model.

analytic results in Section 6 with finite-difference numerical simulations, it is necessary to perform 1-D finite-difference calculations in the transformed domain. This is useful to confirm the validity of the analytic analysis. Comparisons with the 2-D finite-difference calculations in the spatial domain (Section 4) would not be as useful. First, it is difficult to accurately measure amplitudes in the finite-difference results as the pulse shapes are distorted by the curved wave fronts (see Figs 1–4). Secondly, we have the additional approximation of the differentials in the transverse direction in the 2-D finite-difference calculations. The analytic results are in the transformed domain, so the transverse differentials are handled exactly. It is more satisfactory to compare the analytic results with 1-D finite-difference calculations in the transformed domain, where if the discretization is fine enough, the results should be comparable.

The 1-D finite-difference equations in the transformed domain can be derived for the discrete approximation to eq. (38). In the velocity–stress, staggered-grid formulation (Virieux 1986), the stresses are defined on the gridpoints, and the particle velocities are defined on the staggered-gridpoints (or vice versa). The time updates of the particle velocities on the staggered grid depend on central difference approximations of spatial differentials of the stresses [the equation of motion (1)], and the time updates of the stresses on the grid depend on central difference approximations of spatial differentials of the particle velocities (the constitutive eq. 2). Commonly, the time derivative, ∂_t, is approximated by a two-point difference, and the spatial derivatives, ∂_3, by a four-point formula as in Section 4.

In the transformed domain, the Virieux grid is collapsed onto one spatial dimension, x_3, and the grid and staggered-grid variables become mixed. For the transformed, 2-D problems, v_1, σ_{33} and P are defined on the gridpoints and v_3 and σ_{31} on the staggered-gridpoints. Thus, the formula to update the gridpoints is

$$\partial_t \begin{pmatrix} v_1 \\ \sigma_{33} \end{pmatrix} = q_{\mathrm{P}}^{-2} \begin{pmatrix} -p\lambda/\eta & 1/\eta \\ \rho - \xi p^2 & -p\lambda/\eta \end{pmatrix} \partial_3 \begin{pmatrix} v_3 \\ \sigma_{31} \end{pmatrix} \tag{85}$$

from (47), and for the staggered-gridpoints

$$\partial_t \begin{pmatrix} v_3 \\ \sigma_{31} \end{pmatrix} = q_{\mathrm{V}}^{-2} \begin{pmatrix} -p & 1/\mu \\ \rho & -p \end{pmatrix} \partial_3 \begin{pmatrix} v_1 \\ \sigma_{33} \end{pmatrix} \tag{86}$$

omitting the source terms for brevity. Note that the equations have become mixed, and we no longer have a one-to-one correspondence between updating the grid and staggered grid, and the constitutive equations and the equation of motion. On the spatial grid, the variables v_1 and σ_{33} are defined on gridpoints in the temporal grid, and the similarly v_3 and σ_{31} are defined on staggered-gridpoints in space and time. The transverse particle displacement, u_1, required for the source term is calculated from the time integral of v_1 and is known on the spatial grid but the temporal staggered grid.

In the acoustic limit, the equations reduce to

$$\partial_t(-P) = \rho\, q^{-2}\, \partial_3 v_3 \tag{87}$$

for the grid updates, and

$$\partial_t(v_3) = \partial_3(-P)/\rho \tag{88}$$

for the staggered-grid updates, from (50).

The finite-difference calculations are performed using discrete forms of eqs (85) and (86) for the elastic solution, and (87) and (88) for the acoustic solution and its correction. The standard second order in time and fourth order in space, staggered-grid formulation is used, and as outlined above all the required derivatives are compatible with the definitions of the grid and staggered grid.

An example of these 1-D, finite-difference calculations for the acoustic, elastic and corrected solutions is shown in Figs 9 and 10. Fig. 9 shows 15 snapshots of the particle velocity. The source is a minimum-phase Ricker wavelet with a central frequency of 100 Hz. The acoustic, elastic and corrected solutions are shown with a small vertical shift to separate the curves. The direct, incident, reflected and transmitted acoustic and P waves are clearly visible, and in the elastic case, the reflected and transmitted S waves are just visible. To see the details, the final snapshot is replotted in Fig. 10.

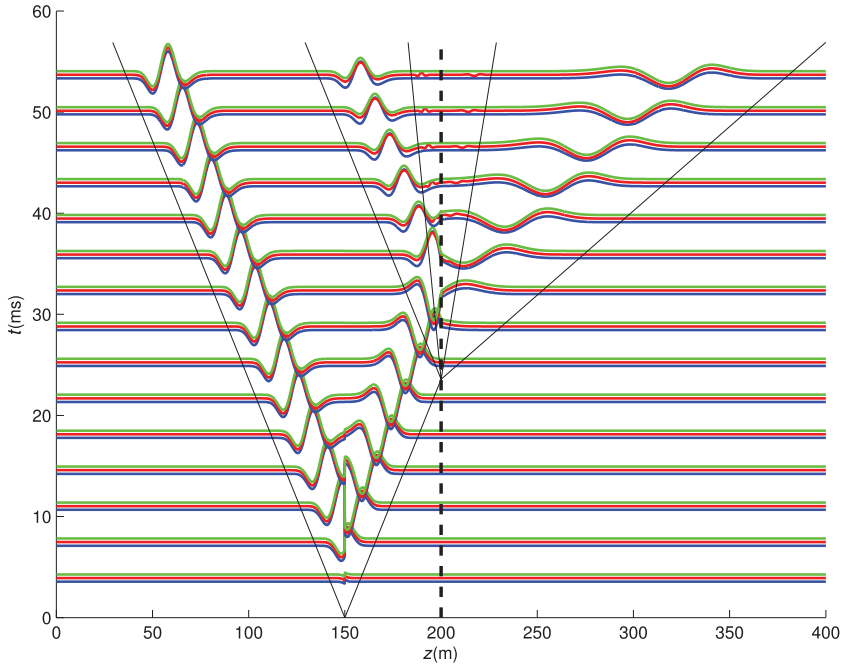

Figure 9. The elastic, acoustic and corrected solutions for the sedimentary model. The record are snapshots of the particle velocity, v_3, at intervals of 3.56 ms. The incident wave angle is 45°. The horizontal axis is z. The plane wave is introduce at $z = 150$ m and the interface is at $z = 200$ m. The colour code is the same as in Figs 2 and 4—blue for the acoustic solution, red for the elastic solution and green for the corrected solution. The pulse is a minimum-phase Ricker wavelet with central frequency of 100 Hz. The traveltimes of the source, reflected and transmitted waves are indicated. To distinguish the curves, the elastic and corrected solutions are shifted vertically by 0.1 and 0.2 of the separation of the snapshots, respectively.

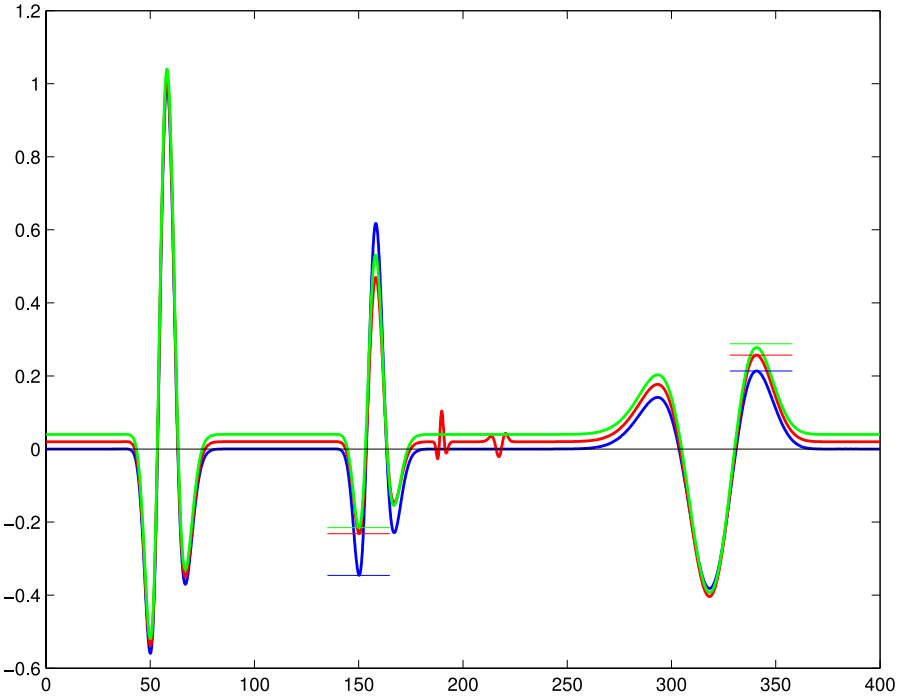

Figure 10. The elastic, acoustic and corrected solutions for the sedimentary model. The record is the snapshot of the particle velocity, v_3, at time 53.4 ms, the final snapshot in Fig. 9. Apart for the scale, other details are as Fig. 9. The theoretical amplitudes for the reflected and transmitted pulses for all solutions, predicted from the amplitude of the incident pulse, are indicated by the horizontal lines. In order to distinguish the curves, the elastic and corrected solutions are shifted vertically by 0.02 and 0.04 units, respectively.

Again the acoustic, elastic and corrected solutions are shown with a small vertical shift to separate the curves. The elastic reflected and transmitted *S* waves are more clearly visible. Taking the first peak amplitude from the direct wave, the predicted amplitudes of the reflected and transmitted waves for the three solutions are indicated with the horizontal lines. The accuracy of the acoustic and elastic finite-difference calculations is evident. Reasonable agreement is obtained for the corrected, reflected and transmitted *P*

waves. The agreement for the acoustic correction is not perfect, but the disagreement is largely due to the numerical approximations involved in the second derivative of u_1^{A} (which is 'discontinuous') in the residual source ($\nabla \cdot \mathbf{e}^{\mathrm{A}}$ in eq. 28). This was confirmed by performing a simulation with $[\rho\,] = 0$ when the contribution from the second derivative is zero [as the coefficient of the delta function in (70), which leads to the delta function derivative in the residual force source, is zero]. Then, the agreement is much improved.

8 CONCLUSIONS

In this paper we developed a theory for correcting the wavefield in acoustic finite-difference simulations for some of the elastic effects in an elastic model. The method works by treating the first acoustic simulation as an approximate solution of the elastic wave equation, and calculating the error in this equation. Introducing the negative of this error as sources in a second acoustic simulation allows calculation of a correction for the acoustic wavefield that simulates some of the elastic effects of the elastic wave equation. In principle the iterative procedure could be continued, but probably the most useful effect is from the first iteration. The calculation of the error terms can be restricted to inhomogeneous regions where waves are reflected or converted, for example, interface regions, making their computation a small additional cost. Although individual terms in the error sources (the residual moment-density elements) are non-zero in homogeneous regions, overall the total error force-equivalent sources are zero, i.e. the moment-density sources are silent in homogeneous regions. The main cost is for the second acoustic simulation. If the error terms are calculated everywhere, the cost will be considerably greater, but still less than the equivalent elastic simulation.

The error terms must be introduced into a separate acoustic simulation. If the errors are introduced immediately as corrections to the original acoustic simulation, then the computations include all aspects of the elastic simulation and become equivalent to elastic simulations on the acoustic grid (as we have confirmed numerically and by analysis). Elastic simulations on the acoustic grid are another possible way to correct acoustic simulations, but have the disadvantage that they will contain dispersed *S* waves and their later conversions to *P* waves.

We demonstrated by finite-difference calculations that the correction procedure significantly improves the amplitudes of reflection *P* waves even at a strong interface between sediment and salt. This correction was confirmed by analytic results for the correction to the plane-wave coefficients, and one-dimensional finite-difference computations for plane waves. In this paper we have only considered the finite-difference method for the simulations, but the iterative procedure could be used with other numerical techniques.

Although we only applied the method to correct acoustic wavefields for the effects of isotropic elasticity, the method is more general and could be applied to correct the solution of one wave equation for effects from another, similar wave equation. For instance, it could be used to correct for anisotropy, if the kinematic properties can be included in an approximate simulation, or attenuation. For transversely isotropic (TI) media, anisotropic approximations for the acoustic equations have been developed that model the kinematic properties of *qP* in TI media reasonably accurately (Duveneck *et al.* 2008, Fowler *et al.* 2010, Bube *et al.* 2012). The approximate anisotropic acoustic simulation can then be corrected for the elastic TI effects using the theory developed in this paper.

The analytic correction for the reflection coefficient (the consitutive relationship 2) is very good (Figs 5 and 7) and may well have other applications, e.g. amplitude-versus-angle studies. In an alternative notation, it can be written

$$\ddot{\mathcal{T}} \simeq \frac{Z_2 \cos\theta_1 - Z_1 \cos\theta_2}{Z_2 \cos\theta_1 + Z_1 \cos\theta_2} + [\mu^{\mathrm{E}}] \left(2\bar{\rho} + \frac{1}{2}[\rho]\right) \frac{\sin 2\theta_1 \sin 2\theta_2}{(Z_2 \cos\theta_1 + Z_1 \cos\theta_2)^2}, \tag{89}$$

where $Z = \rho\alpha$ is the acoustic impedance, and θ is the *P*-ray angle with the normal to the interface.

ACKNOWLEDGEMENTS

We thank Schlumberger for permission to publish this paper, and two anonymous reviewers for their useful comments.

REFERENCES

Backus, G. & Mulcahy, M., 1976. Moment tensor and other phenomenological descriptions of seismic sources—I. Continuous displacements, *Geophys. J. R. astr. Soc.,* **46,** 341–361.

Bube, K.P., Memeth, T., Stefani, J.P., Liu, W., Nihei, K.T., Ergas, R. & Zhang, L., 2012. First-order systems for elastic and acoustic variable-tilt TI media, *Geophysics,* **77,** T157–T170.

Chapman, C.H., 2004. *Fundamentals of Seismic Wave Propagation,* Cambridge Univ. Press.

Duveneck, E., Milcik, P., Bakker, P.M. & Perkins, C., 2008. Acoustic VTI wave equations and their application for anisotropic reverse-time migration, in *Proceedings of 78th Annual International Meeting,* SEG Expanded Abstracts, pp. 2186–2190.

Fowler, P.J., Du, X. & Fletcher, R.P., 2010. Coupled equations for reverse time migration in transversely isotropic media, *Geophsyics,* **75,** S11–S22.

Hobro, J.W.D., Chapman, C.H. & Robertsson, J.O.A., 2014. A method for correcting acoustic finite-difference amplitudes, *Geophysics,* in press.

Levander, A., 1988. Fourth-order finite-difference *P-SV* seismograms, *Geophysics,* **53,** 1425–1436.

Robertsson, J.O.A. & Blanch, J.O., 2011. Numerical methods: finite-difference, in *Encyclopedia of Solid Earth Geophysics,* 2nd edn, pp. 883–892, Springer-Verlag.

Woodhouse, J.H., 1974. Surface waves in a laterally varying layered structure, *Geopys. J. R. astr. Soc.,* **37,** 461–490.

Virieux, J., 1986. *P-SV* wave propagation in heterogeneous media: velocity-stress, finite difference method, *Geophysics,* **51,** 889–901.